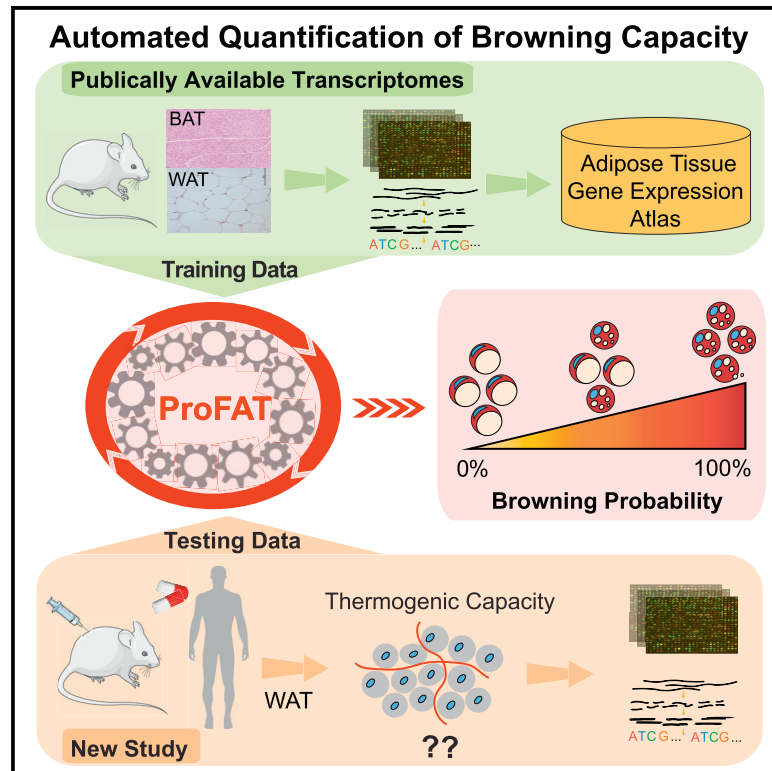


Cell Reports

Prediction of Adipose Browning Capacity by Systematic Integration of Transcriptional Profiles

Graphical Abstract



Authors

Yiming Cheng, Li Jiang, Susanne Keipert, ..., Matthias Tschöp, Martin Jastroch, Fabiana Perocchi

Correspondence

martin.jastroch@helmholtz-muenchen.de (M.J.),
fabiana.perocchi@helmholtz-muenchen.de (F.P.)

In Brief

Cheng et al. develop a computational tool named ProFAT for quantifying the thermogenic potential of mouse and human fat samples based on automated and unbiased prediction of white and brown adipocyte content from raw gene expression datasets. ProFAT is freely available and can be accessed at <http://profat.genzentrum.lmu.de>.

Highlights

- ProFAT represents a resource for exploring adipocyte biology
- ProFAT compiles the largest mouse adipose-centric gene expression atlas
- ProFAT quantifies BAT and WAT content from mouse and human fat transcriptomics
- ProFAT can be freely accessed through a user-friendly interface

Data and Software Availability

GSE112582



Cheng et al., 2018, Cell Reports 23, 3112–3125
June 5, 2018 © 2018 The Author(s).
<https://doi.org/10.1016/j.celrep.2018.05.021>

CellPress

Prediction of Adipose Browning Capacity by Systematic Integration of Transcriptional Profiles

Yiming Cheng,^{1,2,6} Li Jiang,^{1,2,6} Susanne Keipert,^{2,6} Shuyue Zhang,^{1,2} Andreas Hauser,³ Elisabeth Graf,⁴ Tim Strom,⁴ Matthias Tschöp,^{2,5} Martin Jastroch,^{2,*} and Fabiana Perocchi^{1,2,7,*}

¹Gene Center, Department of Biochemistry, Ludwig-Maximilians Universität München, 81377 Munich, Germany

²Institute for Diabetes and Obesity, Helmholtz Diabetes Center, Helmholtz Zentrum München and German National Diabetes Center (DZD), 85764 Neuherberg, Germany

³Laboratory for Functional Genome Analysis (LAFUGA), Gene Center, Ludwig-Maximilians Universität München, 81377 Munich, Germany

⁴Institute of Human Genetics, Helmholtz Zentrum München, 85764 Neuherberg, Germany

⁵Division of Metabolic Diseases, Department of Medicine, Technische Universität München, 80333 Munich, Germany

⁶These authors contributed equally

⁷Lead Contact

*Correspondence: martin.jastroch@helmholtz-muenchen.de (M.J.), fabiana.perocchi@helmholtz-muenchen.de (F.P.)

<https://doi.org/10.1016/j.celrep.2018.05.021>

SUMMARY

Activation and recruitment of thermogenic cells in human white adipose tissues (“browning”) can counteract obesity and associated metabolic disorders. However, quantifying the effects of therapeutic interventions on browning remains enigmatic. Here, we devise a computational tool, named ProFAT (profiling of fat tissue types), for quantifying the thermogenic potential of heterogeneous fat biopsies based on prediction of white and brown adipocyte content from raw gene expression datasets. ProFAT systematically integrates 103 mouse-fat-derived transcriptomes to identify unbiased and robust gene signatures of brown and white adipocytes. We validate ProFAT on 80 mouse and 97 human transcriptional profiles from 14 independent studies and correctly predict browning capacity upon various physiological and pharmacological stimuli. Our study represents the most exhaustive comparative analysis of public data on adipose biology toward quantification of browning after personalized medical intervention. ProFAT is freely available and should become increasingly powerful with the growing wealth of transcriptomics data.

INTRODUCTION

Adipose tissue is broadly divided into white and brown, based on key anatomic, structural, molecular, and metabolic differences (Frontini and Cinti, 2010). White adipose tissue (WAT) is specialized to store chemical energy as fat, whereas brown adipose tissue (BAT) can catabolize lipids and glucose for non-shivering thermogenesis, due to the high mitochondrial mass and expression of uncoupling protein 1 (UCP1), a mitochondrial inner membrane protein that dissipates energy from substrate oxidation directly as heat.

Although major WAT and BAT depots are located in anatomically distinct regions, brown-like, UCP1-positive fat cells can be found sporadically and interspersed in various WAT depots in response to cold exposure or β -adrenergic receptor agonists. These cells have been termed beige, brite (brown-in-white), recruitable or inducible brown, or brown-like adipocytes (Ishibashi and Seale, 2010), owing to their morphological and metabolic features that are similar to “classical” brown adipocytes and to the expression of thermogenic genes (Shabalina et al., 2013). Several studies have suggested that beige adipocytes can derive from bipotential WAT precursors and mature white adipocytes (Barbatelli et al., 2010; Himms-Hagen et al., 2000; Schulz et al., 2011; Wang et al., 2013). However, the structural and functional differences that distinguish them from BAT and WAT still remain unclear.

Advance in positron emission tomography (PET) scanning methods have allowed the discovery that adult humans contain significant deposits of UCP1-positive brown cells in the supraclavicular and neck region (Farmer, 2009) as well as in multiple human WAT depots upon exposure to various physiological and pharmacological effectors (Cypess et al., 2013; Jespersen et al., 2013; Lidell et al., 2013). Promoting the appearance of thermogenic cells in non-classical BAT locations can increase energy expenditure and substrate metabolism, improve glucose tolerance, and correct hyperlipidemia, leading to a healthier metabolic phenotype in both rodents (Bartelt et al., 2011; Min et al., 2016; Stanford et al., 2013) and humans (Saito et al., 2009). Quantifying the browning potential of therapeutic interventions on human BAT activation would therefore accelerate the identification of therapeutic avenues to reduce obesity and its comorbidities. However, this remains challenging, given that human fat contains only a small fraction of brown and brown-like adipocytes.

Lineage-tracing studies for the selective isolation of different adipose cell types have been performed in mice (Bartelt and Heeren, 2014) but are not possible in humans. Furthermore, currently available imaging methods have a limited sensitivity, and the resulting data are difficult to deconvolute. Besides, there are only a handful of adipose tissue marker genes, which have



only been used so far to make a qualitative distinction between human adipocytes or adipose tissue types. Those markers originate from either analyses of whole adipose tissue depots, containing a great proportion of contaminating cells, or *ex vivo* stable and clonally derived adipocytes (Cypess et al., 2013; Shinoda et al., 2015; Wu et al., 2012), which are affected by *in vitro* cell culture conditions. Therefore, novel approaches for the unbiased quantification of browning capacity in patients' fat depots are required.

Here, we take advantage of the wealth of data on global transcriptional profiling of fat depots published over the last decade to develop a robust and automated computational pipeline, which we call ProFAT (profiling of fat tissue types), for the systematic prediction of mouse and human adipose browning capacity based on raw gene expression data (Figure 1). First, we identify a molecular signature of brown and white adipocytes by integrating 51 and 52 global transcriptional profiles of mouse BAT and WAT from seven independent studies, respectively. Next, we develop a computational model trained on all 103 datasets and show that it can correctly classify over 80 additional mouse BAT and WAT samples from nine published studies. Importantly, the model can estimate the degree of browning for WAT-treated samples (beige) independently from biological and technical differences in the anatomical location of fat depots and in experimental models and procedures. We also confirm that our model can be applied to humans and predict the browning capacity of 96 samples derived from heterogeneous tissue biopsies and *ex vivo* immortalized adipocytes. ProFAT is freely available (<http://profat.genzentrum.lmu.de>) and allows users to automatically perform hierarchical clustering (HC), principal-component analysis (PCA), and prediction of browning capacity from raw microarray and RNA sequencing (RNA-seq) datasets.

RESULTS

A Comprehensive Mouse-Adipocyte-Centered Gene Expression Atlas

To compile a comprehensive and unbiased gene expression atlas of mouse fat, we systematically retrieved whole-genome transcriptomes from microarray and RNA-seq studies on adipose tissue biopsies and differentiated clonal adipocytes that are publicly available in GEO and ArrayExpress databases. A total of 16 independent studies on at least two clearly defined adipocytes, for example, classical brown, white, and inducible brown adipocytes (beige or brite), were selected for downstream computational analyses (Baboota et al., 2015; Fang et al., 2015; Fitzgibbons et al., 2011; Grimaldi et al., 2010; Long et al., 2014; Majka et al., 2010; Ohno et al., 2012; Rosell et al., 2014; Seale et al., 2007; Sharp et al., 2012; Su et al., 2004; Timmons et al., 2007; Wang et al., 2016; Wu et al., 2012; Xue et al., 2009; Zhang et al., 2014; Table S1; Figure 2A). Those included 174 microarray and 34 RNA-seq datasets of high reads quality and correlation between biological replicates (Figures S1 and S2), of which 83 were gene expression datasets on a variety of white fat depots originating from different anatomical locations, such as epididymal, inguinal, gonadal, perivascular, mesenteric, and subcutaneous WAT (Figure 2B).

In addition, it contains 63 gene expression datasets on interscapular BAT and 52 on beige or brite adipocytes originated from different WAT depots in response to treatments such as cold, PPAR-gamma agonists (rosiglitazone, fexaramine, forskolin, and roscovitine), and beta-3 adrenergic receptor agonists (CL316,243; Figures 2A and 2B).

Gene Expression Signatures of Brown, White, and Beige or Brite Fat

To construct a global adipose-tissue-centered gene expression map, we aggregated transcriptional profiles from all microarray or RNA-seq-based studies in our atlas (Figure 1). First, spurious differences in gene expression between studies, due to technical variation in array platforms and sequencing libraries, were resolved by correcting for batch effects. Next, PCA (Figure 2C) and HC (Figures S3 and S4) were applied to evaluate the relatedness between transcriptional profiles of BAT, WAT, and beige or brite-depots-derived datasets from all studies. Both approaches highlighted a strong and robust gene expression signature from BAT- and WAT-derived samples, despite their heterogeneous composition. On the whole-genome transcriptional level, the variation between WAT depots, due for example to different anatomical regions, proportion of distinct adipocytes, age, food, and gender, had no relevant contribution to the global WAT signature. Furthermore, the gene expression signatures of BAT and WAT were always clearly distinct, independently from the sequencing method (microarray versus RNA-seq), reflecting robust transcriptional differences in the regulation of their physiology and metabolism. Surprisingly, perivascular WAT (pvWAT) samples from study M9 (Fitzgibbons et al., 2011) showed a molecular signature indistinguishable from BAT-derived samples. This result is fully consistent with findings by Fitzgibbons et al. that thoracic pvWAT from mice fed either a normal or high-fat diet has virtually identical gene expression profiles to brown adipocytes.

With the exception of samples from Wang et al. (2016) (study M13), the transcriptional profile of beige or brite adipocytes from other studies was not clearly distinct from either WAT or BAT groups in both PCA and HC analyses (Figures 2C, S3, and S4). For example, gene expression profiles of beige or brite samples from inguinal WAT (iWAT) biopsies of C57BL6 male mice kept in cold for 1–5 weeks (study M8; Xue et al., 2009) were similar to that of BAT samples in the atlas, grouping together in both PCA and HC analyses. On the contrary, beige or brite samples from subcutaneous (sWAT) and mesenteric (mWAT) WAT biopsies of SV129 female mice kept in cold for 10 days (study M10; Rosell et al., 2014) showed a gene expression signature similar to WAT samples from the same as well as from other studies. Similarly, beige or brite adipocytes from cold acclimated (study R1; Long et al., 2014) and fexaramine-stimulated (study R2) iWAT and gonadal WAT (gWAT) (Fang et al., 2015) clustered with WAT samples from other RNA-seq studies in the atlas, whereas beige or brite adipocytes from iWAT treated with rosiglitazone (study R3; Sharp et al., 2012) grouped with BAT samples.

Taken together, our systematic analysis of transcriptomic data from many published studies highlights robust gene expression differences between BAT and WAT that are independent of experimental procedures, sample purity, origin of fat

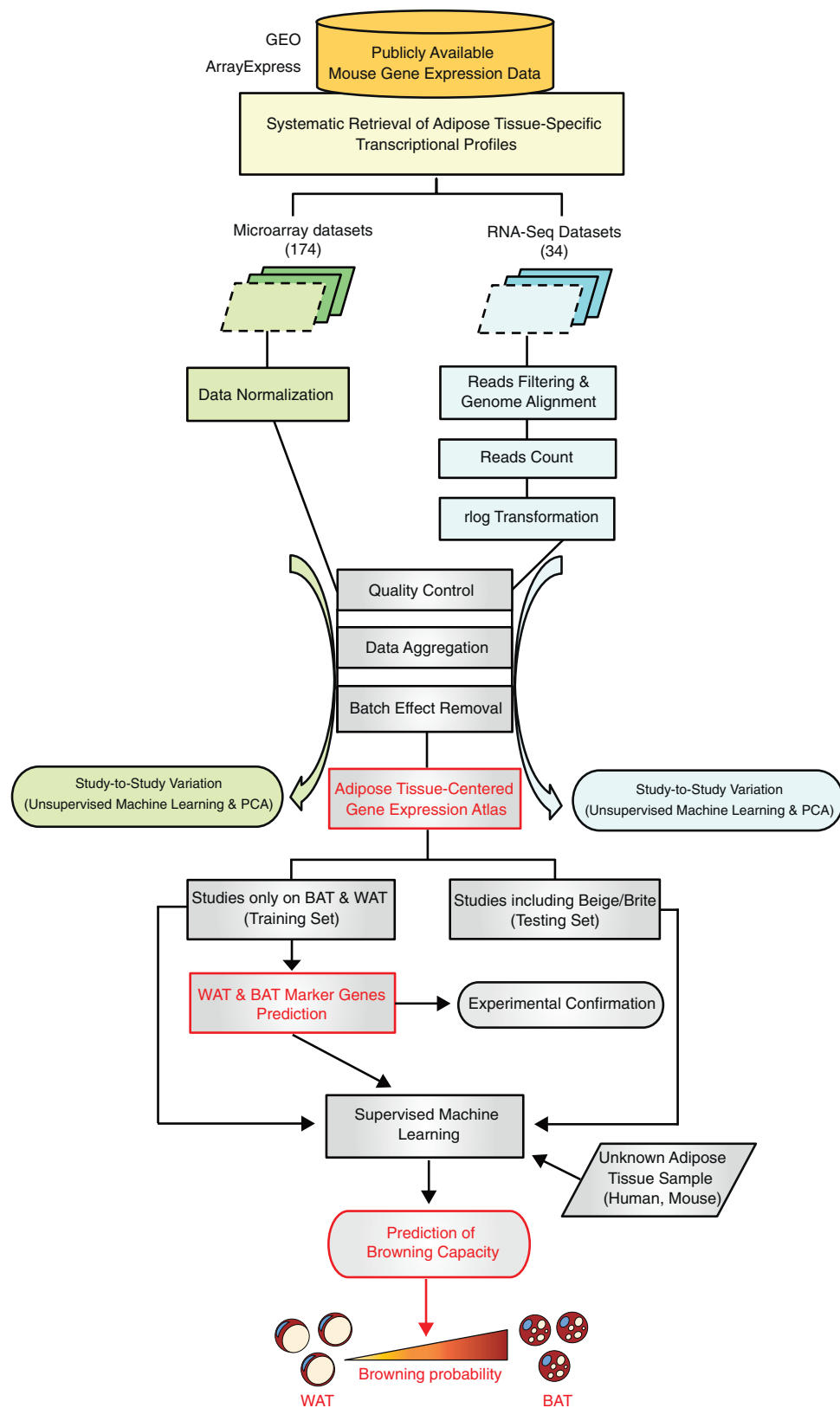


Figure 1. Pipeline for the Systematic and Unbiased Prediction of Adipose Browning Capacity

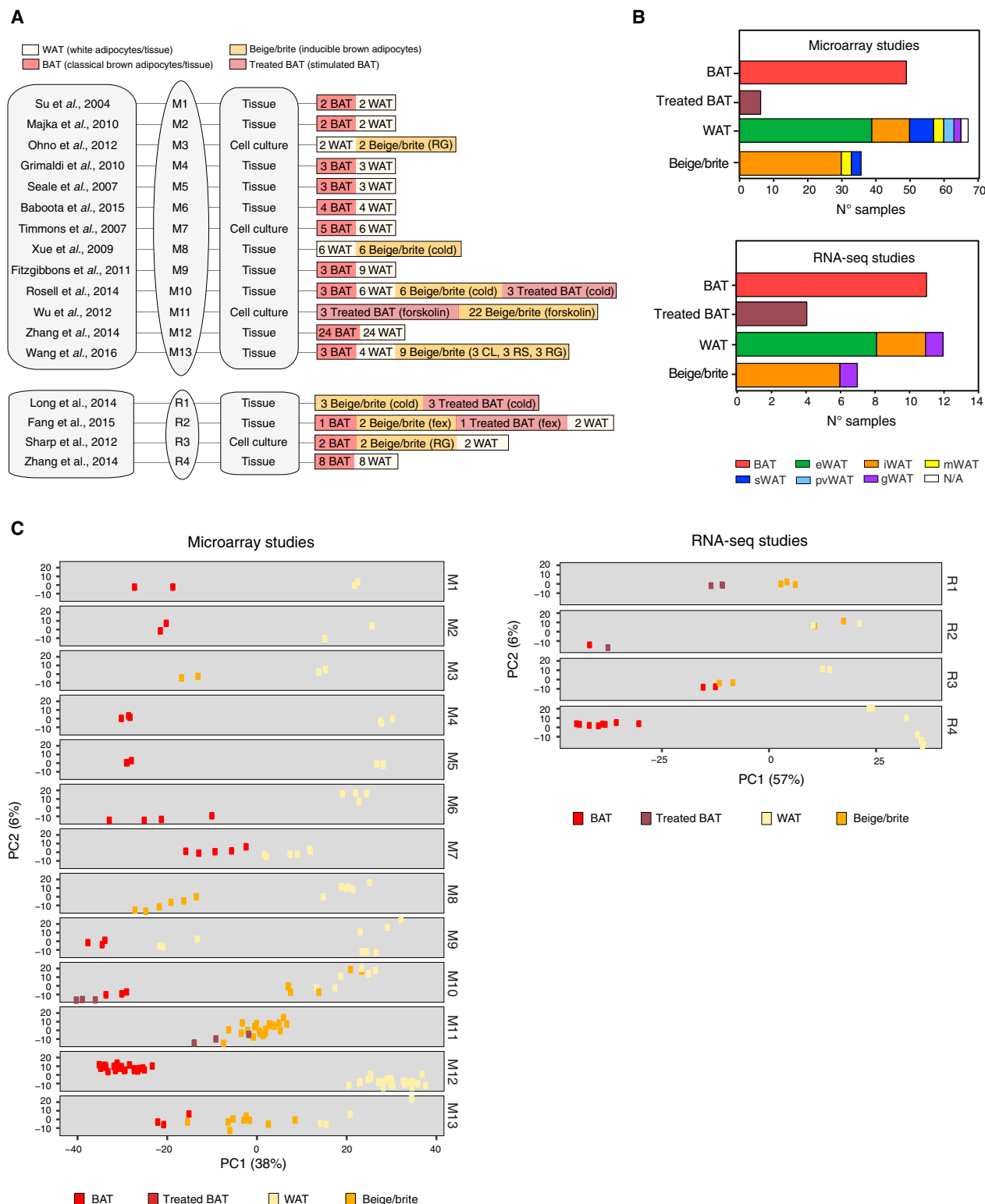


Figure 2. Mouse-Adipocyte-Centered Gene Expression Atlas

(A) Summary of microarray (M1–M13) and RNA-seq studies (R1–R4) on fat samples included in the mouse-adipocyte-centered gene expression atlas. The number of samples for each adipose tissue type within a study is indicated. The stimulus applied to induce browning of WAT (beige or brite) is specified in parentheses (CL, CL316,243; fex, fexamine; RG, rosiglitazone; RS, roscovitine).

(legend continued on next page)

depots, and sequencing methods and can therefore be used to predict an unbiased molecular signature of BAT and WAT.

Prediction of BAT and WAT Molecular Signatures

As a first step toward the prediction of brown adipocytes content (browning capacity) in whole adipose tissue depots, we identified marker genes for classical brown and white fat tissue classification (Figure 3). To this goal, we integrated 51 BAT and 52 WAT transcriptional profiles from seven out of 16 independent studies in our atlas (M1, M2, M4, M5, M6, M7, and M12 and R4 in Figure 2A). Data normalization and batch effect removal were performed to ensure that differences in gene expression intensities were indeed due to differential expression between BAT and WAT sample groups. Ideally, brown and white fat-specific markers should show an “absolute” difference in expression to allow a clear distinction between BAT and WAT, independently of biological differences in fat depots, sample composition (pure populations versus whole tissue biopsies), and their expression in other cell types. Overall, we found a total of 59 genes (Figure 3A) that were consistently and significantly differentially expressed between all BAT and WAT samples (\log_2 fold change > 1.5 and p -adj value < 0.01). We identified several known brown fat markers, such as *Ucp1*, *Cidea* (cell death-inducing DFFA-like effector a), *Cox7a1* (cytochrome c oxidase subunit VII a polypeptide 1), and *Zic1* (zinc finger protein of the cerebellum 1), as well as white fat markers (e.g., *Hoxc8* [transcription factor homeobox C8]). Due to the high abundance of mitochondria in BAT, brown fat markers included several mitochondrial-targeted proteins that are related to mitochondrial biogenesis and metabolism (Calvo et al., 2016). Not surprisingly, our marker core set was enriched in biological processes and pathways that are known to be involved in energy production and glucose and lipid metabolism (Figure 3B).

To further evaluate the predicted marker set, we looked for functional associations between the 59 marker genes (Figure 3C). We employed a computational method, called iRegulon, to reverse engineer the transcriptional regulatory network underlying our set of differentially expressed marker genes. iRegulon searches for *cis*-regulatory regions at 10–20 kb around the transcription start site (TSS) of each gene and then it looks for enrichment in any of ~10,000 transcription factor (TF) motifs from seven different databases and chromatin immunoprecipitation (ChIP)-seq peaks associated with potential TFs. We identified four key TFs targeting 39 out of the 59 markers, which were also differentially expressed between WAT and BAT samples (\log_2 fold change > 1.5 and p value < 0.01). Those included two well-known key adipogenic TFs and co-regulators described in mammals, which are part of the subfamily of peroxisome proliferator-activated receptors (*Ppara* α , peroxisome proliferator-activated receptor alpha; *Ppargc1*, peroxisome proliferator-activated receptor gamma coactivator 1-alpha; Alvarez-Dominguez et al., 2015). Another gene, *Nr4a1* (nuclear receptor

subfamily 4, group A, member 1; also known as NUR77), was previously involved in the control of *Ucp1* expression (Kanzleiter et al., 2005). In addition, we identified *Gata6*, a member of the GATA factors family. Although those factors are generally considered as negative regulators of adipogenesis, *Gata6* has not yet been implicated in the regulation of adipogenesis in mammals (Bou et al., 2017). Next, to validate the predicted BAT and WAT molecular signatures, we quantified the expression of each marker gene in interscapular BAT and iWAT isolated from 16-week-old female mice kept at either thermoneutrality or cold acclimated for two weeks at 18°C, followed by 4 weeks at 5°C, in order to induce browning (Figure S5). We confirmed that all of our brown fat markers were indeed highly expressed in classical BAT from both room temperature and cold-exposed mice (Figures 3D and S6). The expression of many of those markers, such as *Ucp1*, *Cidea*, *Cox7a1*, and *Pdk4*, was also higher in WAT from cold-exposed mice than in untreated WAT, reflecting the induction of browning; instead, others appeared to be brown specific (e.g., *Zic1*, *Impdh1*, *Tmem246*, and *Shmt1*). Similar results were obtained with male mice of the same age and background (data not shown). Notably, several genes have not yet been associated to BAT (*Aco2*, *Gm13910*, and *Acaa2*) and WAT (*Alcam*, *Ar*, *Sgpp1*, and *Gria3*) and could therefore represent novel BAT and WAT markers.

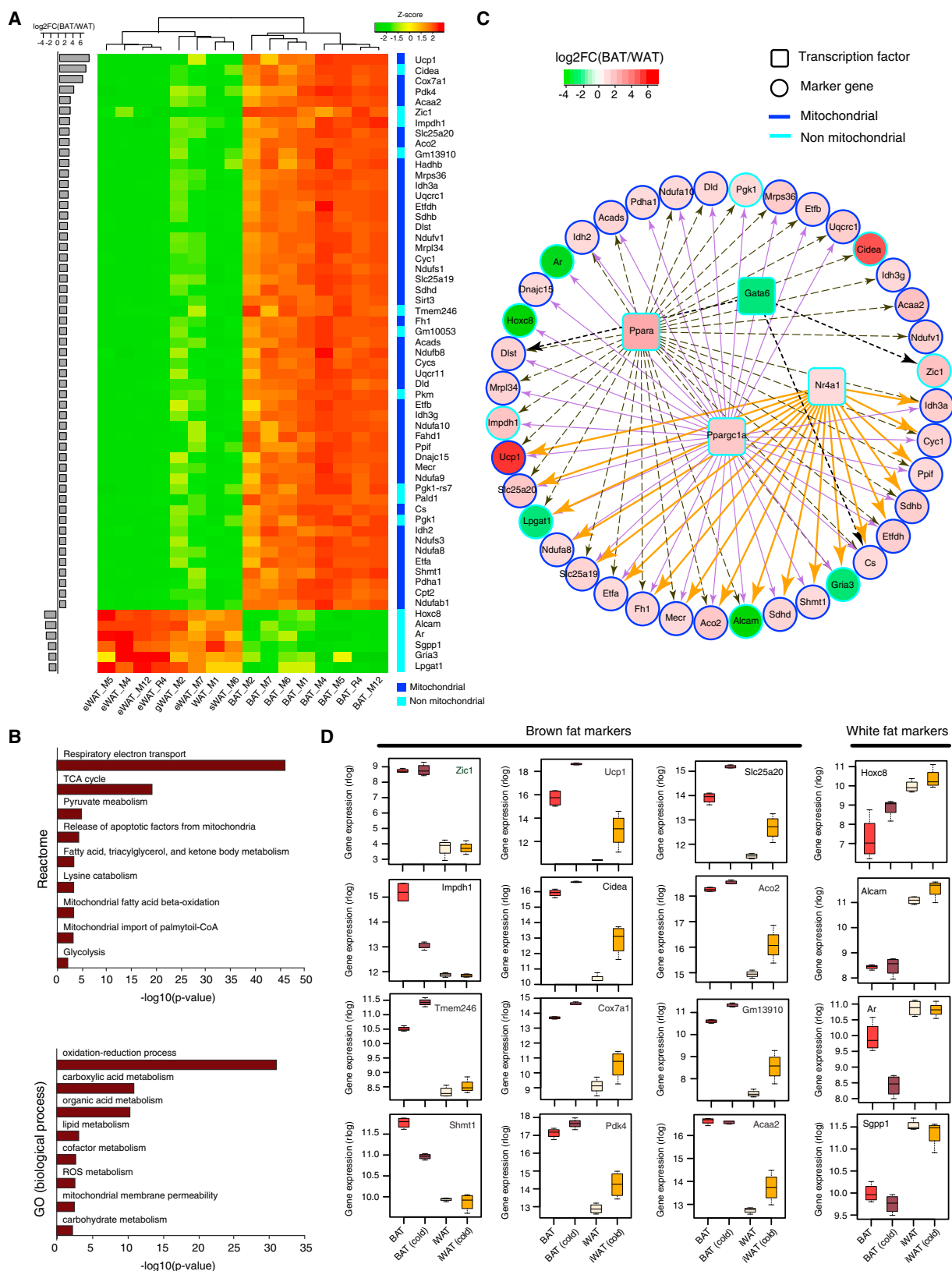
Automated Prediction of Mouse Adipose Tissue Browning Capacity

To assess the thermogenic potential of fat tissues in response to browning agents, we devised a computational model that can predict brown and white adipocytes content (“BAT probability”; probability to be brown-like) independently of sample purity and experimental systems (Figure 4A). The model combines into a single-layer neural network (SLNN) the transcriptional profiles of 51 BAT and 52 WAT samples from M1, M2, M4, M5, M6, M7, M12, and R4, which represent our “training set,” and the predicted core marker set. Our choice of SLNN was justified by a systematic comparison to the performance of other algorithms, such as random forest, naive Bayes, generalized linear model, recursive partitioning, and support vector machine (Figure S7). To this goal, each machine learning algorithm was first trained through a leave-one-out cross-validation (LOOCV) step, and the accuracy of different models was then assessed based on the correct classification of BAT and WAT samples from a “testing set” of nine independent studies (M3, M8, M9, M10, M11, M13, R1, R2, and R3). As shown in Figure S7, SLNN outperformed other algorithms and was therefore employed for follow-up analyses.

Next, we tested the predictive power of our model using transcriptomes of white adipocytes from primary cell culture, whole fat tissue biopsies, as well as immortalized clonal lines, in which thermogenesis was activated by either cold, rosiglitazone (RG), roscovitine (RS), CL316,243 (CL), forskolin, or fexaramine (fex)

(B) Sample distribution among different adipose tissue types in all microarray and RNA-seq studies. eWAT, epididymal white adipose tissue; gWAT, gonadal white adipose tissue; iWAT, inguinal white adipose tissue; mWAT, mesenteric white adipose tissue; N/A, not specified; pvWAT, perivascular white adipose tissue; sWAT, subcutaneous white adipose tissue.

(C) Study-by-study principle-component analysis (PCA) of normalized gene expression data. See also Table S1 and Figures S1–S4.



(legend on next page)

treatment (Figures 4B and S8). The model deconvolutes the percentage of brown adipocytes (thermogenic cells) and calculates the probability that a specific sample has acquired a brown-like transcriptional signature. A browning probability close to 0% and 100% would indicate a fat sample with WAT-like and BAT-like profiles, respectively. Instead, a browning probability close to 50% would suggest either that the tissue profile is neither BAT- nor WAT-like (e.g., de-differentiated adipocytes and other tissue types) or that it has features of both fat types (e.g., it consists of an equal mixture of brown and white adipocytes).

As shown in Figure 4B, our model always classifies BAT and WAT with almost 100% accuracy and predicts the thermogenic potential of beige or brite samples to be higher than the corresponding untreated WAT samples, a result that is in agreement with the relative UCP1 expression level measured in each sample. A “positive control” in our analysis is represented by study M9. Here, the model “misclassifies” samples from pvWAT as having a high browning probability, thus BAT-like. However, our prediction is fully consistent with findings from the original study of Fitzgibbons et al. (2011), showing a virtually identical molecular signature between pvWAT and BAT from mice fed either a normal or high-fat diet. Notably, cold-treated sWAT from study M10 showed both a high UCP1 expression level and browning capacity, whereas the model predicted the same treatment to be ineffective when applied to mWAT. This result is consistent with previous observations that rodents’ sWAT depots are more sensitive to acquisition of BAT characteristics and have a higher thermogenic potential than visceral depots, such as mWAT (Seale et al., 2011; Tiraby and Langin, 2003). When we applied our model on datasets from study M13, we found that samples defined by Wang et al. (2016) to originate from BAT and iWAT had a browning capacity close to 100% and 0%, respectively. Reassuringly, treatment of iWAT with the browning agent CL was predicted to yield a strong increase in browning capacity, in accordance with results from functional analyses. Similarly, we found that the thermogenic potential of CL-based iWAT treatment was higher than either RG or RS. Accordingly, measurements of rectal temperature in mice that were exposed to cold after treatment with each browning agent showed that the starting body temperature of CL-treated mice was the highest and CL was the most potent enhancer of glucose tolerance among all three drugs. Moreover, HC analysis also confirmed that, at the transcriptional level, UCP1-positive adipocytes arising in WAT of mice treated with RG and RS were more similar to each other than to UCP1-positive cells from CL-treated mice, which showed a transcriptome very close to that of BAT. Accordingly, RS- and RG-treated cells expressed several fold lower levels of *Ucp1* than cells from BAT and

CL-treated adipocytes. We also obtained consistent results between our predictions and functional characterizations of fex-treated and untreated iWAT and gWAT from study R2. Here, the model predicted that fex treatment would not result in an increased browning activity of WAT. This is in agreement with the low *Ucp1* level measured in those samples and with observations that fex-treated mice show reduction in weight gain and improved metabolic homeostasis upon diet-induced obesity, which was largely attributed to enhanced thermogenic activity in BAT rather than browning of iWAT or gWAT. However, the significance of our prediction is difficult to assess for this study, given that only one replicate for each sample is available.

Overall, our predictions are in agreement with HC analyses, but whereas those can only provide a qualitative classification of each sample, our model can also estimate its thermogenic potential in response to a variety of browning stimuli.

Automated Prediction of Human Adipose Tissue Browning Capacity

To evaluate the applicability of our mouse-based model to deconvolute browning capacity of heterogeneous adipocyte populations from human samples, we retrieved publicly available transcriptomics analyses of human adipose tissues (Table S1; Figures 5A and S9). Those included a total of 97 datasets from 3 microarray and 2 RNA-seq-based studies on a variety of different experimental models: immortalized clonal preadipocyte cell lines derived from stromal vascular fractions (SVFs) of subcutaneous and deep neck of four adult human subjects (study hM1; Xue et al., 2015); primary adipocytes isolated from paired biopsies of deep and subcutaneous neck adipose tissue from six patients undergoing neck surgery (study hM2; Tews et al., 2014); adipose tissue isolated from abdominal subcutaneous fat depots of seven type 2 diabetic (T2D) patients before and after 10 days of cold acclimation (study hM3; Hanssen et al., 2015); pluripotent stem cell (PSC)-derived white (WAs) and brown (BAs) adipocytes subjected to the Janus kinase 3 (JAK3) and spleen tyrosine kinase (SYK) inhibitors tofacitinib and R406, respectively (study hR1; Moisan et al., 2015); and immortalized clonal brown and white preadipocytes isolated from SVFs in supraclavicular BAT and sWAT of two adult humans before and after *in vitro* differentiation and in response to forskolin treatment (study hR2; Shinoda et al., 2015). All of these studies were used as “testing set” in the neural network model (Figure 5B), which was trained on BAT and WAT samples from mouse-specific studies, as previously shown in Figure 4A. Each testing dataset was first mapped through orthology to mouse genes. Overall, we observed that the level of *UCP1* expression in the original datasets was not always correlating to the browning

Figure 3. Prediction and Validation of BAT and WAT Marker Genes

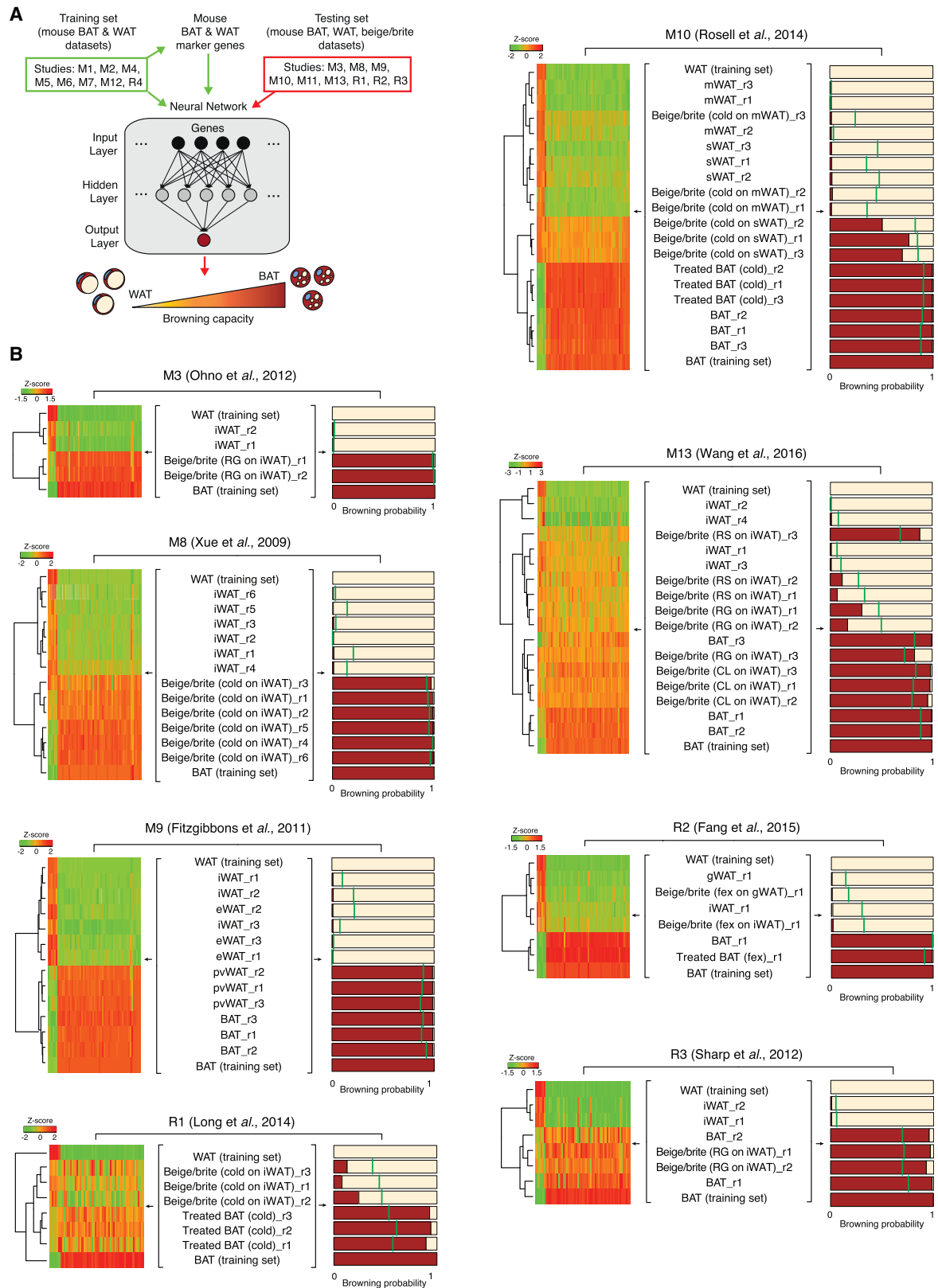
(A) Relative gene expression changes (Z score) for the predicted marker genes (53 and 6 BAT and WAT markers, respectively). MitoCarta2 is used to predict mitochondrial localization of marker genes.

(B) Gene Ontology (GO) and pathway (Reactome) enrichment analysis of marker genes.

(C) Transcriptional regulatory network of BAT and WAT marker genes (circles) and predicted targeting transcription factors (squares). Nodes are colored based on the \log_2 fold change of the average expression level in BAT and WAT samples used for markers prediction (\log_2 FC > 1.5 and p-adj value < 0.01).

(D) Experimental validation of BAT and WAT marker genes ($n \geq 4$). On each box, central line and edges represent median and 25th and 75th percentiles, respectively, and the whiskers extend to the most extreme data points.

See also Figures S5 and S6.



(legend on next page)

capacity predicted by our model. Overall, we found *UCP1* to be a weak classifier of brown- versus white-like depots, particularly when analyzing human tissue biopsies. Our observation is in agreement with previous claims that the thermogenic potential of human adipose tissues does not directly correlate with the simple presence of *UCP1*-positive cells (Rosenwald et al., 2013). Whereas *UCP1* expression can be used as a marker of active brown adipocytes, in heterogeneous populations, it would be insufficient to estimate brown adipocyte content. Therefore, we evaluated the predictive value of our model in human samples where *UCP1* level could not be used to quantify browning. As an example, Tews et al. (2014) (study hM2) looked for functional differences between paired adipose tissue biopsies from deep neck, where human BAT is commonly found, and subcutaneous neck, where WAT is enriched. Accordingly, our model predicted higher browning capacity in samples from deep compared to subcutaneous neck, despite minor changes in *UCP1* expression level measured by microarray analysis. Interestingly, based on our prediction, the deep neck samples of some patients showed stronger browning capacity than others, possibly reflecting biological variations in BAT content or technical differences in the depth of tissue biopsies between individuals. In another study by Hanssen et al. (2015; study hM3), chronic cold exposure was employed in seven human patients with T2D as a possible strategy to improve glucose homeostasis. Cold acclimation was previously shown to increase supraclavicular BAT mass and activity and to lead to recruitment of *UCP1*-positive adipocytes in other adipose tissue depots. Accordingly, all subjects showed an increase in cold-induced glucose uptake rate in the supraclavicular BAT region, although quite different between the individuals. However, BAT activity and mass were unaffected in other fat depots, such as sWAT and visceral WAT, and no sign of browning could be detected by microarray-based gene expression analysis of abdominal sWAT biopsies from the same patients before and after cold acclimation. Consistently, we also found that the browning capacity of sWAT from each patient was unaffected by cold acclimation, given that there was a minor difference in browning probability between sWAT samples before and after cold exposure. These results are in agreement with findings from multiple studies showing that cold does not brown all human fat depots equally (Conere et al., 1986; Leitner et al., 2017; Romu et al., 2016; Vosselman et al., 2014). Findings from our model applied to hR1 datasets were also in agreement with observations in the original study by Moisan et al. (2015). Here, the JAK3 and SYK inhibitors, tofacitinib and R406, respectively, were shown to induce browning of human PSC-WAs. When comparing the browning probability of PSC-WAs samples treated with DMSO, R406, or tofacitinib, our model correctly predicted a drug-dependent increase in

browning. We also predicted a much higher browning capacity for R406 (PSC-WAs SYKi) than for tofacitinib (PSC-WAs JAK3)-treated adipocytes, which was consistent with evidence of higher *UCP1* and *FABP4* (fatty acid binding protein 4) expression, small lipid droplet area, and mitochondrial content in response to R406. Our data also suggested that both SYK and JAK3 inhibitors are more potent browning inducers than cell fate conversion methods, as shown by comparing the BAT probability of PSC-derived brown adipocytes (PSC-BAs) with PSC-WAs. Finally, when testing samples from study hR2, we found that preadipocytes from supraclavicular and subcutaneous fat depots showed very low browning capacity, which increased after differentiation to brown, but not to white adipocytes, respectively. As expected, a cyclic AMP (cAMP) stimulus induced by treatment with forskolin increased the browning probability of sWAT-derived clonal lines, also confirmed by the activation of thermogenic markers observed in Shinoda et al. (2015).

Altogether, these results demonstrate that our mouse-based model can be also applied to quantify white and brown adipocytes content in *ex vivo* clonally derived human adipocytes and complex human biopsies and to reliably predict the thermogenic potential of treatments applied to induce browning of white fat depots.

DISCUSSION

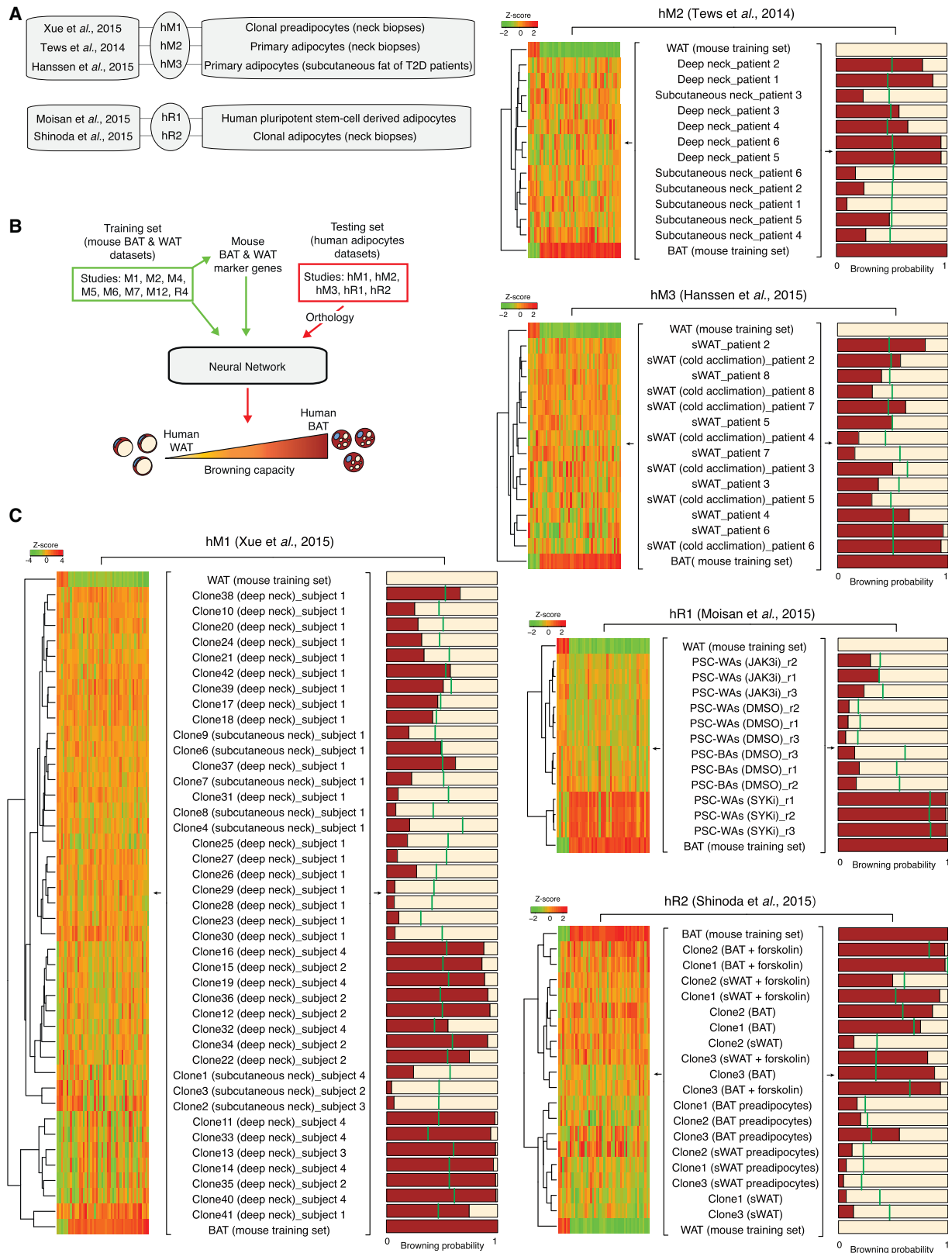
Integrative data analyses have been extensively shown to outperform the predictive power of individual large-scale studies (Calvo et al., 2006; Liu, 2005; Pagliarini et al., 2008; Perocchi et al., 2006). Therefore, when combining multiple datasets from different and complementary approaches, we can learn more about the system than what would be gained by analyzing each dataset in isolation. Given the wealth of transcriptional analyses in the field of adipose biology, obesity, and its comorbidities, we found it timely to perform a meta-analysis of published data and combine into a single framework the knowledge acquired from each study so far. To this goal, we compiled the largest adipose-centric gene expression atlas and developed ProFAT, a systematic and automated approach to derive a robust and unbiased molecular signature of mouse BAT and WAT. This was then used to train a computational model in quantifying the browning capacity of heterogeneous fat tissues in both mouse and humans. We found that BAT and WAT show clearly distinct molecular signatures, irrespective of the anatomical location of the fat depots, their cell types composition, experimental models, and procedures employed. Instead, when we applied ProFAT to several transcriptomics data from beige samples, we observed that the extent to which beige or brite fat differs from either WAT or BAT greatly depends on

Figure 4. Prediction of Browning Capacity of Mouse Adipose Tissue Samples from Test Studies by Supervised Machine Learning

(A) Schematic diagram of the supervised machine learning approach.

(B) Estimation of browning capacity in samples from each test study (right). HC analysis based on relative gene expression changes (Z score) of marker genes is shown for all samples and biological replicates within each test study (left). The green line on each bar represents the sample's relative *Ucp1* gene expression level calculated as $(\text{sample_Ucp1} - \min_Ucp1) / (\max_Ucp1 - \min_Ucp1)$, where the \min_Ucp1 and \max_Ucp1 indicate the minimum and the maximum value of *Ucp1* gene expression across test and training sets, respectively. BAT (training set), combined BAT samples from all training datasets; r, replicates; WAT (training set), combined WAT samples from all training datasets.

See Table S1 for detailed description of each sample. See also Figures S7 and S8.



(legend on next page)

study-to-study differences. Indeed, the degree of browning may vary due to samples purity, length, and type (cold, PPAR- γ , or beta-3 adrenergic receptor agonists) of browning stimuli and to whether the fat sample derives from tissue biopsies, primary adipocytes, or clonal cell populations. The latter can be affected by *in vitro* adaptations, culture microenvironments, and cell-cell interactions. Unsupervised clustering analyses of gene expression data from pure clonally derived beige adipocytes have suggested that those could be classified as a distinct fat type at the transcriptional level (Wu et al., 2012). Whereas our analysis cannot formally rule out a distinct origin of beige from either brown or white adipocytes, it prompts for caution when defining beige-specific signatures in the context of a few limited dataset and biological models, rather than either systematically across a large and diverse set of data or based on pure populations of UCP1-positive cells (Wang et al., 2016).

The computational pipeline developed in this study will be especially important when trying to evaluate the thermogenic potential of therapeutic approaches in humans. Human adipose tissue biopsies usually yield limiting amounts of sample to perform an exhaustive functional characterization of browning, and classical BAT markers, like *UCP1*, have been shown to be insufficient to predict adipose tissue types. Instead, whole-genome expression analyses typically require little material to be performed and have become a method of choice to infer functional remodeling of WATs, based on the assumption that the phenotype is reflected in the gene expression signature. Our meta-analysis enables to classify complex tissue samples from distinct fat depots as well as from *in vitro* derived adipocytes of both mouse and humans, based on their relative brown and white-like molecular signatures. We envision a scenario in which medical researchers can directly assess the thermogenic potential of the patient's white fat sample, prior to and post-medical intervention.

Finally, we generate a user-friendly interface where microarray and RNA-seq-based datasets from mouse and human samples can be directly uploaded and analyzed with both HC and PCA methods, and their browning probability can be automatically computed using ProFAT. This resource can be freely accessed and should become increasingly powerful with the growing wealth of transcriptomics data.

EXPERIMENTAL PROCEDURES

Systematic Retrieval of Adipose-Tissue-Specific Transcriptional Profiles

NCBI GEO and EBI ArrayExpress databases published before September 1, 2015 were queried using the following keywords: "adipocyte," "adipose white," "adipose brown," "adipose beige," "fat white," "fat brown," "fat beige," "BAT," and "WAT." Systematic retrieval of whole genome expression profiles for *Mus musculus* and *Homo sapiens* from NCBI GEO and EBI

ArrayExpress databases was performed through the Entrez Programming Utilities (E-utilities) and programmatic access, respectively. The GEOquery package from Bioconductor (Davis and Meltzer, 2007) was used to retrieve raw CEL microarray data. Only microarray and RNA-seq datasets generated with Affymetrix and Illumina HiSeq Series sequencing platforms, respectively, were considered for downstream computational analyses.

Data Processing

Raw CEL microarray data were normalized by quantile normalization using the robust multiarray average (RMA) function in affy (Gautier et al., 2004) and oligo (Carvalho and Irizarry, 2010) R packages. Probe IDs were mapped to Ensembl gene IDs using BiomaRt (Durinck et al., 2009) based on the following criteria: probes not mapping to any gene ID were excluded; probes mapping to multiple gene IDs were assigned to all genes; and for probes mapping to the same gene ID, the mean expression value was considered.

Processing of raw FastQ files from RNA-seq analyses involved three main steps. First, adapters, barcodes, and sequences with a Phred quality scores below 20 were removed using the Trim Galore software. Second, raw reads were mapped against mouse or human reference genomes (Ensembl release 81) using TopHat v2.0.13 (Trapnell et al., 2009) with Bowtie index (Bowtie 2.2.0.0) and GTF transcript annotation files. Next, the number of reads mapping to each Ensembl gene ID were counted using the ht-seq count software (Anders et al., 2015) to obtain raw read counts and quantify gene expression. A gene was defined as expressed if the sum of raw read counts across all datasets within a study was >1. Last, DESeq2 (regularized logarithm transformation algorithm; Love et al., 2014) was used to perform rlog transformation (conversion of raw read counts in \log_2 scale), which minimizes differences between samples and normalize with respect to library size.

For each study, a data matrix was generated, whereby each row and column corresponded to an Ensembl gene ID and sample ID, respectively. Correlation analyses were performed using pheatmap R package based on a pairwise distance matrix generated using Euclidean distance. Biological replicates that did not replicate were considered as outliers and removed from follow-up analyses. Data from all microarray or RNA-seq-based studies were aggregated based on gene IDs and then combat algorithm (Johnson et al., 2007) was applied to remove the batch effect across multiple batches of microarray and RNA-seq experiments and to calculate normalized gene expression values. This algorithm is robust to outliers in small sample sizes and performs comparable to existing methods for large samples. Hierarchical clustering was performed using Euclidean distance and complete linkage based on normalized gene expression values. Differential gene expression analysis was performed using the Limma algorithm, and significantly differentially expressed genes were defined based on an adjusted p values < 0.01 and a mean \log_2 fold-change threshold >1.5.

Identification of BAT and WAT Marker Genes

Microarray and RNA-seq gene expression data on BAT and WAT samples from the following studies M1, M2, M4, M5, M6, M7, M12, and R4 were combined based on Gene IDs. Combat algorithm (Johnson et al., 2007) was applied to remove batch effects and to calculate normalized gene expression values. Next, the MGFM (Marker Gene Finder in MicroArray) bioinformatics tool (El Amrani et al., 2015) was applied to predict genes that allow a robust and specific segregation of samples from BAT and WAT types (<http://www.bioconductor.org/packages/release/bioc/html/MGFM.html>; default parameters). The subset of 59 genes that were significantly differentially expressed (\log_2 fold-change > 1.5 and p-adj value < 0.01) was selected as a core BAT and WAT marker set. The ConsensusPathDB-Mouse (<http://cpdb.molgen.mpg.de/MCPDB>) was used to identify non-redundant functional categories

Figure 5. Prediction of Browning Capacity of Human Adipose Tissue Samples by Supervised Machine Learning

(A) Summary of microarray (hM1–3) and RNA-seq studies (hR1–2) on human fat samples.

(B) Schematic diagram of the supervised machine learning approach.

(C) Estimation of browning capacity (right) and HC analysis (left) of samples from each human-adipocytes-based study. JAK3i, Janus kinase 3 inhibitor (tofacitinib); PSC-BAs, pluripotent stem cell-derived brown adipocytes; PSC-WAs, pluripotent stem cell derived white adipocytes; SYKi, spleen tyrosine kinase inhibitor (R406).

See Table S1 for detailed description of each sample. See also Figure S9.

from Gene Ontology (GO) and Reactome that were enriched within BAT and WAT marker genes (p value < 0.01). Cytoscape (Shannon et al., 2003) was used to display the predicted regulatory network.

In-House RNA-Seq

Total RNA was extracted from inguinal WAT and interscapular BAT of 16-week-old female C57BL/6 mice kept either for the whole life at an ambient temperature of 30°C or for two weeks at 18°C followed by 4 weeks at 5°C ($n = 4$; not randomization and blinding applied). Qiazol was used for RNA extraction according to the manufacturer's instructions (Qiazol Lysis Reagent; QIAGEN). The quality of the RNA was determined with the Agilent 2100 BioAnalyzer (RNA 6000 Nano Kit; Agilent Technologies). All samples had a RNA integrity number (RIN) value greater than 8. For library preparation, 1 μ g of total RNA per sample was used. RNA molecules were poly(A) selected, fragmented, and reverse transcribed with the Elute, Prime, Fragment Mix (EPF; Illumina). End repair, A-tailing, adaptor ligation, and library enrichment were performed as described in the low-throughput protocol of the TruSeq RNA Sample Prep Guide (Illumina). RNA libraries were assessed for quality and quantity with the Agilent 2100 BioAnalyzer and the Quant-iT PicoGreen dsDNA Assay Kit (Life Technologies). RNA libraries were sequenced as 100-bp paired-end runs on an Illumina HiSeq2500 platform. The animal welfare authorities approved animal maintenance and experimental procedures.

Prediction of Adipose Tissue Browning Capacity by Machine Learning

A neural network model was developed with one hidden layer, using caret R package with method set to nnet. Leave-one-out cross validation was used to tune the number of hidden units and weight decay, whereas default values were used for the remaining parameters. Datasets were exclusively assigned to either a test or a training group. The training data only included datasets from study M1, M2, M4, M5, M6, M7, M12, and R4. Instead, the test data included microarray and RNA-seq datasets from study M3, M8, M9, M10, M11, M13, R1, R2, and R3. To avoid introducing circularity in the analysis, test data were independent from training data and were never used for training. COMBAT algorithm was applied to normalize any new test dataset against the training set in order to remove batch effects, and then the training set together with the core marker set were used in the neural network. Human transcriptional profiles were also used as testing set by mapping human gene IDs to mouse ortholog gene IDs with BioMart (Ensembl release 81) restricted to ortholog_one2one mapping type.

Statistical Analysis

Z score is calculated as $(X - \mu)/\sigma$, where X is the value of the element, μ is the mean, and σ is the SD. A marker gene is defined significant if the adjusted p value < 0.01 and the $\log_2(\text{fold change}) > 1.5$, where p value and fold change are calculated with DESeq R package.

DATA AND SOFTWARE AVAILABILITY

The accession number for in-house RNA-seq data reported in this paper is GEO: GSE112582. The data and code can be accessed at <https://github.com/PerocchiLab/ProFAT>. Accession codes for publicly available microarray and RNA-seq datasets used in this study are also listed in Table S1.

SUPPLEMENTAL INFORMATION

Supplemental Information includes nine figures and one table and can be found with this article online at <https://doi.org/10.1016/j.celrep.2018.05.021>.

ACKNOWLEDGMENTS

We acknowledge support from the German Research Foundation (DFG) under the Emmy Noether Programme (PE 2053/1-1) and the Bavarian Ministry of Sciences, Research and the Arts in the framework of the Bavarian Molecular Biosystems Research Network (D2-F5121.2–10c/4822) to F.P., Y.C., and L.J.

AUTHOR CONTRIBUTIONS

Conceptualization, F.P. and M.J.; Methodology, Y.C., S.K., and L.J.; Software, Y.C., A.H., and L.J.; Formal Analysis, Y.C., A.H., L.J., and T.S.; Investigation, S.K. and E.G.; Resources, F.P., M.J., and M.T.; Data Curation, S.K. and S.Z.; Writing – Original Draft, F.P., M.J., S.K., and Y.C.; Visualization, F.P., L.J., Y.C., and A.H.; Supervision, F.P. and M.J.; Funding Acquisition, F.P.

DECLARATION OF INTERESTS

The authors declare no competing interests.

Received: December 28, 2017

Revised: March 6, 2018

Accepted: May 2, 2018

Published: June 5, 2018

REFERENCES

- Alvarez-Dominguez, J.R., Bai, Z., Xu, D., Yuan, B., Lo, K.A., Yoon, M.J., Lim, Y.C., Knoll, M., Slavov, N., Chen, S., et al. (2015). De novo reconstruction of adipose tissue transcriptomes reveals long non-coding RNA regulators of brown adipocyte development. *Cell Metab.* 21, 764–776.
- Anders, S., Pyl, P.T., and Huber, W. (2015). HTSeq—a Python framework to work with high-throughput sequencing data. *Bioinformatics* 31, 166–169.
- Baboota, R.K., Sarma, S.M., Boparai, R.K., Kondepudi, K.K., Mantri, S., and Bishnoi, M. (2015). Microarray based gene expression analysis of murine brown and subcutaneous adipose tissue: significance with human. *PLoS ONE* 10, e0127701.
- Barbatelli, G., Murano, I., Madsen, L., Hao, Q., Jimenez, M., Kristiansen, K., Giacobino, J.P., De Matteis, R., and Cinti, S. (2010). The emergence of cold-induced brown adipocytes in mouse white fat depots is determined predominantly by white to brown adipocyte transdifferentiation. *Am. J. Physiol. Endocrinol. Metab.* 298, E1244–E1253.
- Bartelt, A., and Heeren, J. (2014). Adipose tissue browning and metabolic health. *Nat. Rev. Endocrinol.* 10, 24–36.
- Bartelt, A., Bruns, O.T., Reimer, R., Hohenberg, H., Ilttrich, H., Peldschus, K., Kaul, M.G., Tromsdorf, U.I., Weller, H., Waurisch, C., et al. (2011). Brown adipose tissue activity controls triglyceride clearance. *Nat. Med.* 17, 200–205.
- Bou, M., Montfort, J., Le Cam, A., Ralli  re, C., Lebre  t, V., Gabillard, J.C., Weil, C., Guti  rrez, J., Rescan, P.Y., Capilla, E., and Navarro, I. (2017). Gene expression profile during proliferation and differentiation of rainbow trout adipocyte precursor cells. *BMC Genomics* 18, 347.
- Calvo, S., Jain, M., Xie, X., Sheth, S.A., Chang, B., Goldberger, O.A., Spinazola, A., Zeviani, M., Carr, S.A., and Mootha, V.K. (2006). Systematic identification of human mitochondrial disease genes through integrative genomics. *Nat. Genet.* 38, 576–582.
- Calvo, S.E., Clauser, K.R., and Mootha, V.K. (2016). MitoCarta2.0: an updated inventory of mammalian mitochondrial proteins. *Nucleic Acids Res.* 44 (D1), D1251–D1257.
- Carvalho, B.S., and Irizarry, R.A. (2010). A framework for oligonucleotide microarray preprocessing. *Bioinformatics* 26, 2363–2367.
- Conere, T.J., Church, S.W., and Lowry, W.S. (1986). The radioprotective role of common anaesthetic and other narcotic agents. *Radiother. Oncol.* 5, 347–348.
- Cypess, A.M., White, A.P., Vernochet, C., Schulz, T.J., Xue, R., Sass, C.A., Huang, T.L., Roberts-Toler, C., Weiner, L.S., Sze, C., et al. (2013). Anatomical localization, gene expression profiling and functional characterization of adult human neck brown fat. *Nat. Med.* 19, 635–639.
- Davis, S., and Meltzer, P.S. (2007). GEOquery: a bridge between the Gene Expression Omnibus (GEO) and BioConductor. *Bioinformatics* 23, 1846–1847.
- Durincik, S., Spellman, P.T., Birney, E., and Huber, W. (2009). Mapping identifiers for the integration of genomic datasets with the R/Bioconductor package biomaRt. *Nat. Protoc.* 4, 1184–1191.

- El Amrani, K., Stachelscheid, H., Lekschas, F., Kurtz, A., and Andrade-Navarro, M.A. (2015). MGFM: a novel tool for detection of tissue and cell specific marker genes from microarray gene expression data. *BMC Genomics* 16, 645.
- Fang, S., Suh, J.M., Reilly, S.M., Yu, E., Osborn, O., Lackey, D., Yoshihara, E., Perino, A., Jacinto, S., Lukasheva, Y., et al. (2015). Intestinal FXR agonism promotes adipose tissue browning and reduces obesity and insulin resistance. *Nat. Med.* 21, 159–165.
- Farmer, S.R. (2009). Obesity: be cool, lose weight. *Nature* 458, 839–840.
- Fitzgibbons, T.P., Kogan, S., Aouadi, M., Hendricks, G.M., Straubhaar, J., and Czech, M.P. (2011). Similarity of mouse perivascular and brown adipose tissues and their resistance to diet-induced inflammation. *Am. J. Physiol. Heart Circ. Physiol.* 301, H1425–H1437.
- Frontini, A., and Cinti, S. (2010). Distribution and development of brown adipocytes in the murine and human adipose organ. *Cell Metab.* 11, 253–256.
- Gautier, L., Cope, L., Bolstad, B.M., and Irizarry, R.A. (2004). affy-analysis of Affymetrix GeneChip data at the probe level. *Bioinformatics* 20, 307–315.
- Grimaldi, B., Bellet, M.M., Katada, S., Astarita, G., Hirayama, J., Amin, R.H., Granneman, J.G., Piomelli, D., Leff, T., and Sassone-Corsi, P. (2010). PER2 controls lipid metabolism by direct regulation of PPAR γ . *Cell Metab.* 12, 509–520.
- Hanssen, M.J., Hoeks, J., Brans, B., van der Lans, A.A., Schaart, G., van den Driessche, J.J., Jörgensen, J.A., Boekschoten, M.V., Hesselink, M.K., Havkes, B., et al. (2015). Short-term cold acclimation improves insulin sensitivity in patients with type 2 diabetes mellitus. *Nat. Med.* 21, 863–865.
- Himms-Hagen, J., Melnyk, A., Zingaretti, M.C., Ceresi, E., Barbatelli, G., and Cinti, S. (2000). Multilocular fat cells in WAT of CL-316243-treated rats derive directly from white adipocytes. *Am. J. Physiol. Cell Physiol.* 279, C670–C681.
- Ishibashi, J., and Seale, P. (2010). Medicine. Beige can be slimming. *Science* 328, 1113–1114.
- Jespersen, N.Z., Larsen, T.J., Pejts, L., Dagaard, S., Homøe, P., Loft, A., de Jong, J., Mathur, N., Cannon, B., Nedergaard, J., et al. (2013). A classical brown adipose tissue mRNA signature partly overlaps with brite in the supraclavicular region of adult humans. *Cell Metab.* 17, 798–805.
- Johnson, W.E., Li, C., and Rabinovic, A. (2007). Adjusting batch effects in microarray expression data using empirical Bayes methods. *Biostatistics* 8, 118–127.
- Kanzleiter, T., Schneider, T., Walter, I., Bolze, F., Eickhorst, C., Heldmaier, G., Klaus, S., and Klingenspor, M. (2005). Evidence for Nr4a1 as a cold-induced effector of brown fat thermogenesis. *Physiol. Genomics* 24, 37–44.
- Leitner, B.P., Huang, S., Brychta, R.J., Duckworth, C.J., Baskin, A.S., McGehee, S., Tal, I., Dieckmann, W., Gupta, G., Kolodny, G.M., et al. (2017). Mapping of human brown adipose tissue in lean and obese young men. *Proc. Natl. Acad. Sci. USA* 114, 8649–8654.
- Lidell, M.E., Betz, M.J., Dahlqvist Leinhard, O., Heglind, M., Elander, L., Slawik, M., Mussack, T., Nilsson, D., Romu, T., Nuutila, P., et al. (2013). Evidence for two types of brown adipose tissue in humans. *Nat. Med.* 19, 631–634.
- Liu, E.T. (2005). Systems biology, integrative biology, predictive biology. *Cell* 121, 505–506.
- Long, J.Z., Svensson, K.J., Tsai, L., Zeng, X., Roh, H.C., Kong, X., Rao, R.R., Lou, J., Lokurkar, I., Baur, W., et al. (2014). A smooth muscle-like origin for beige adipocytes. *Cell Metab.* 19, 810–820.
- Love, M.I., Huber, W., and Anders, S. (2014). Moderated estimation of fold change and dispersion for RNA-seq data with DESeq2. *Genome Biol.* 15, 550.
- Majka, S.M., Fox, K.E., Psilas, J.C., Helm, K.M., Childs, C.R., Acosta, A.S., Janssen, R.C., Friedman, J.E., Woessner, B.T., Shade, T.R., et al. (2010). De novo generation of white adipocytes from the myeloid lineage via mesenchymal intermediates is age, adipose depot, and gender specific. *Proc. Natl. Acad. Sci. USA* 107, 14781–14786.
- Min, S.Y., Kady, J., Nam, M., Rojas-Rodríguez, R., Berkenwald, A., Kim, J.H., Noh, H.L., Kim, J.K., Cooper, M.P., Fitzgibbons, T., et al. (2016). Human 'brite/beige' adipocytes develop from capillary networks, and their implantation improves metabolic homeostasis in mice. *Nat. Med.* 22, 312–318.
- Moisan, A., Lee, Y.K., Zhang, J.D., Hudak, C.S., Meyer, C.A., Prummer, M., Zoffmann, S., Truong, H.H., Ebeling, M., Kiialainen, A., et al. (2015). White-to-brown metabolic conversion of human adipocytes by JAK inhibition. *Nat. Cell Biol.* 17, 57–67.
- Ohno, H., Shinoda, K., Spiegelman, B.M., and Kajimura, S. (2012). PPAR γ agonists induce a white-to-brown fat conversion through stabilization of PRDM16 protein. *Cell Metab.* 15, 395–404.
- Pagliarini, D.J., Calvo, S.E., Chang, B., Sheth, S.A., Vafai, S.B., Ong, S.E., Walford, G.A., Sugiana, C., Boneh, A., Chen, W.K., et al. (2008). A mitochondrial protein compendium elucidates complex I disease biology. *Cell* 134, 112–123.
- Perocchi, F., Jensen, L.J., Gagneur, J., Ahting, U., von Mering, C., Bork, P., Prokisch, H., and Steinmetz, L.M. (2006). Assessing systems properties of yeast mitochondria through an interaction map of the organelle. *PLoS Genet.* 2, e170.
- Romu, T., Vavrukh, C., Dahlqvist-Leinhard, O., Tallberg, J., Dahlström, N., Persson, A., Heglind, M., Lidell, M.E., Enerbäck, S., Borga, M., and Nystrom, F.H. (2016). A randomized trial of cold-exposure on energy expenditure and supraclavicular brown adipose tissue volume in humans. *Metabolism* 65, 926–934.
- Rosell, M., Kafrou, M., Frontini, A., Okolo, A., Chan, Y.W., Nikolopoulou, E., Millership, S., Fenech, M.E., MacIntyre, D., Turner, J.O., et al. (2014). Brown and white adipose tissues: intrinsic differences in gene expression and response to cold exposure in mice. *Am. J. Physiol. Endocrinol. Metab.* 306, E945–E964.
- Rosenwald, M., Perdikari, A., Rülcke, T., and Wolfrum, C. (2013). Bi-directional interconversion of brite and white adipocytes. *Nat. Cell Biol.* 15, 659–667.
- Saito, M., Okamatsu-Ogura, Y., Matsushita, M., Watanabe, K., Yoneshiro, T., Nio-Kobayashi, J., Iwanaga, T., Miyagawa, M., Kameya, T., Nakada, K., et al. (2009). High incidence of metabolically active brown adipose tissue in healthy adult humans: effects of cold exposure and adiposity. *Diabetes* 58, 1526–1531.
- Schulz, T.J., Huang, T.L., Tran, T.T., Zhang, H., Townsend, K.L., Shadrach, J.L., Cerletti, M., McDougall, L.E., Giorgadze, N., Tchonia, T., et al. (2011). Identification of inducible brown adipocyte progenitors residing in skeletal muscle and white fat. *Proc. Natl. Acad. Sci. USA* 108, 143–148.
- Seale, P., Kajimura, S., Yang, W., Chin, S., Rohas, L.M., Uldry, M., Tavernier, G., Langin, D., and Spiegelman, B.M. (2007). Transcriptional control of brown fat determination by PRDM16. *Cell Metab.* 6, 38–54.
- Seale, P., Conroe, H.M., Estall, J., Kajimura, S., Frontini, A., Ishibashi, J., Cohen, P., Cinti, S., and Spiegelman, B.M. (2011). Prdm16 determines the thermogenic program of subcutaneous white adipose tissue in mice. *J. Clin. Invest.* 121, 96–105.
- Shabalina, I.G., Petrovic, N., de Jong, J.M., Kalinovich, A.V., Cannon, B., and Nedergaard, J. (2013). UCP1 in brite/beige adipose tissue mitochondria is functionally thermogenic. *Cell Rep.* 5, 1196–1203.
- Shannon, P., Markiel, A., Ozier, O., Baliga, N.S., Wang, J.T., Ramage, D., Amin, N., Schwikowski, B., and Ideker, T. (2003). Cytoscape: a software environment for integrated models of biomolecular interaction networks. *Genome Res.* 13, 2498–2504.
- Sharp, L.Z., Shinoda, K., Ohno, H., Scheel, D.W., Tomoda, E., Ruiz, L., Hu, H., Wang, L., Pavlova, Z., Gilsanz, V., and Kajimura, S. (2012). Human BAT possesses molecular signatures that resemble beige/brite cells. *PLoS ONE* 7, e49452.
- Shinoda, K., Luijten, I.H., Hasegawa, Y., Hong, H., Sonne, S.B., Kim, M., Xue, R., Chondronikola, M., Cypess, A.M., Tseng, Y.H., et al. (2015). Genetic and functional characterization of clonally derived adult human brown adipocytes. *Nat. Med.* 21, 389–394.
- Stanford, K.I., Middelbeek, R.J., Townsend, K.L., An, D., Nygaard, E.B., Hitchcox, K.M., Markan, K.R., Nakano, K., Hirshman, M.F., Tseng, Y.H., and Goodyear, L.J. (2013). Brown adipose tissue regulates glucose homeostasis and insulin sensitivity. *J. Clin. Invest.* 123, 215–223.

- Su, A.I., Wiltshire, T., Batalov, S., Lapp, H., Ching, K.A., Block, D., Zhang, J., Soden, R., Hayakawa, M., Kreiman, G., et al. (2004). A gene atlas of the mouse and human protein-encoding transcriptomes. *Proc. Natl. Acad. Sci. USA* *101*, 6062–6067.
- Tews, D., Schwar, V., Scheithauer, M., Weber, T., Fromme, T., Klingenspor, M., Barth, T.F., Möller, P., Holzmann, K., Debatin, K.M., et al. (2014). Comparative gene array analysis of progenitor cells from human paired deep neck and subcutaneous adipose tissue. *Mol. Cell. Endocrinol.* *395*, 41–50.
- Timmons, J.A., Wennmalm, K., Larsson, O., Walden, T.B., Lassmann, T., Petrovic, N., Hamilton, D.L., Gimeno, R.E., Wahlestedt, C., Baar, K., et al. (2007). Myogenic gene expression signature establishes that brown and white adipocytes originate from distinct cell lineages. *Proc. Natl. Acad. Sci. USA* *104*, 4401–4406.
- Tiraby, C., and Langin, D. (2003). Conversion from white to brown adipocytes: a strategy for the control of fat mass? *Trends Endocrinol. Metab.* *14*, 439–441.
- Trapnell, C., Pachter, L., and Salzberg, S.L. (2009). TopHat: discovering splice junctions with RNA-Seq. *Bioinformatics* *25*, 1105–1111.
- Vosselman, M.J., Vijgen, G.H., Kingma, B.R., Brans, B., and van Marken Lichtenbelt, W.D. (2014). Frequent extreme cold exposure and brown fat and cold-induced thermogenesis: a study in a monozygotic twin. *PLoS ONE* *9*, e101653.
- Wang, Q.A., Tao, C., Gupta, R.K., and Scherer, P.E. (2013). Tracking adipogenesis during white adipose tissue development, expansion and regeneration. *Nat. Med.* *19*, 1338–1344.
- Wang, H., Liu, L., Lin, J.Z., Aprahamian, T.R., and Farmer, S.R. (2016). Browning of white adipose tissue with roscovitine induces a distinct population of UCP1⁺ adipocytes. *Cell Metab.* *24*, 835–847.
- Wu, J., Boström, P., Sparks, L.M., Ye, L., Choi, J.H., Giang, A.H., Khandekar, M., Virtanen, K.A., Nuutila, P., Schaart, G., et al. (2012). Beige adipocytes are a distinct type of thermogenic fat cell in mouse and human. *Cell* *150*, 366–376.
- Xue, Y., Petrovic, N., Cao, R., Larsson, O., Lim, S., Chen, S., Feldmann, H.M., Liang, Z., Zhu, Z., Nedergaard, J., et al. (2009). Hypoxia-independent angiogenesis in adipose tissues during cold acclimation. *Cell Metab.* *9*, 99–109.
- Xue, R., Lynes, M.D., Dreyfuss, J.M., Shamsi, F., Schulz, T.J., Zhang, H., Huang, T.L., Townsend, K.L., Li, Y., Takahashi, H., et al. (2015). Clonal analyses and gene profiling identify genetic biomarkers of the thermogenic potential of human brown and white preadipocytes. *Nat. Med.* *21*, 760–768.
- Zhang, R., Lahens, N.F., Ballance, H.I., Hughes, M.E., and Hogenesch, J.B. (2014). A circadian gene expression atlas in mammals: implications for biology and medicine. *Proc. Natl. Acad. Sci. USA* *111*, 16219–16224.

Cell Reports, Volume 23

Supplemental Information

Prediction of Adipose Browning

Capacity by Systematic Integration

of Transcriptional Profiles

Yiming Cheng, Li Jiang, Susanne Keipert, Shuyue Zhang, Andreas Hauser, Elisabeth Graf, Tim Strom, Matthias Tschöp, Martin Jastroch, and Fabiana Perocchi

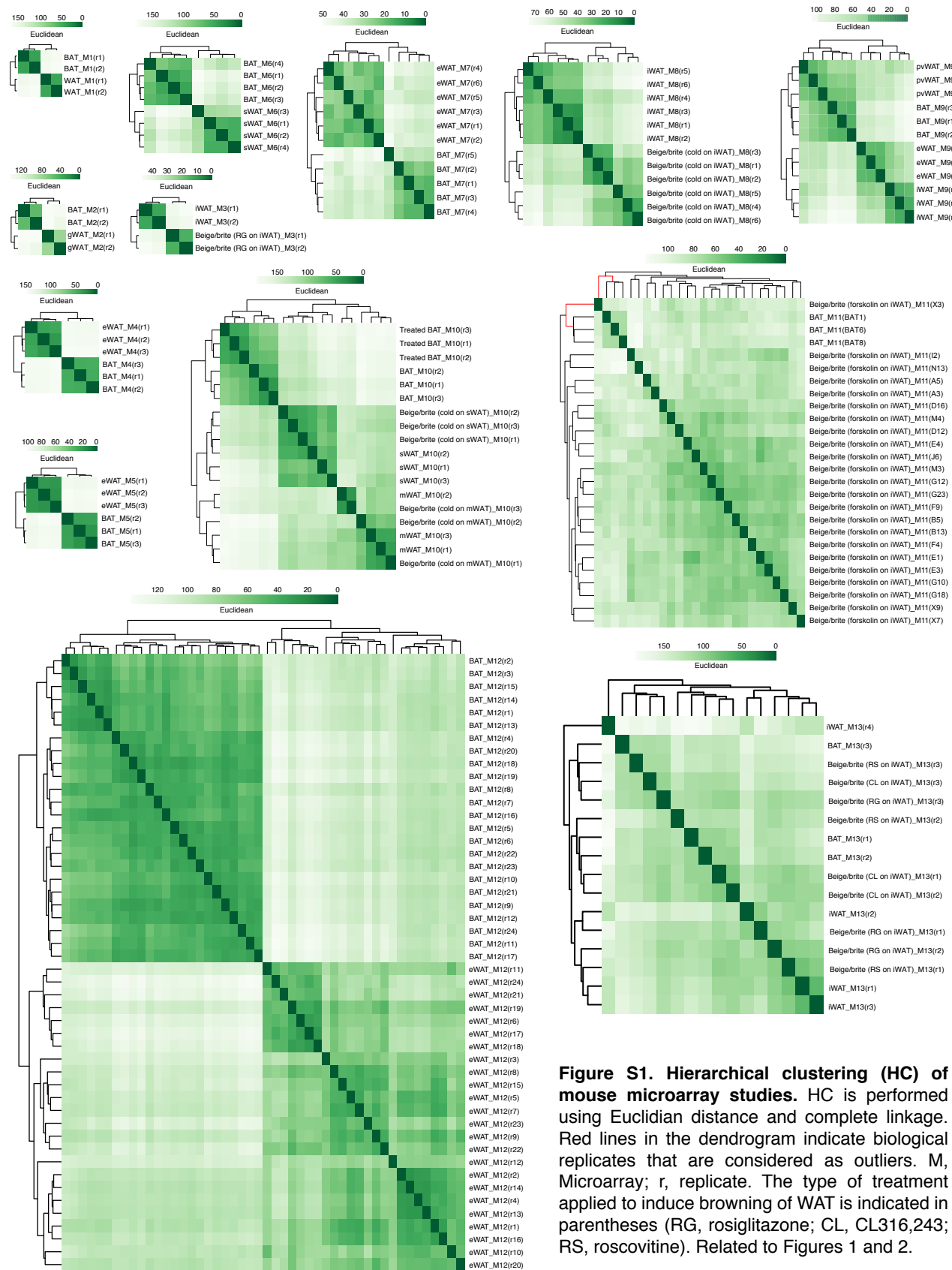


Figure S1. Hierarchical clustering (HC) of mouse microarray studies. HC is performed using Euclidian distance and complete linkage. Red lines in the dendrogram indicate biological replicates that are considered as outliers. M, Microarray; r, replicate. The type of treatment applied to induce browning of WAT is indicated in parentheses (RG, rosiglitazone; CL, CL316,243; RS, roscovitine). Related to Figures 1 and 2.

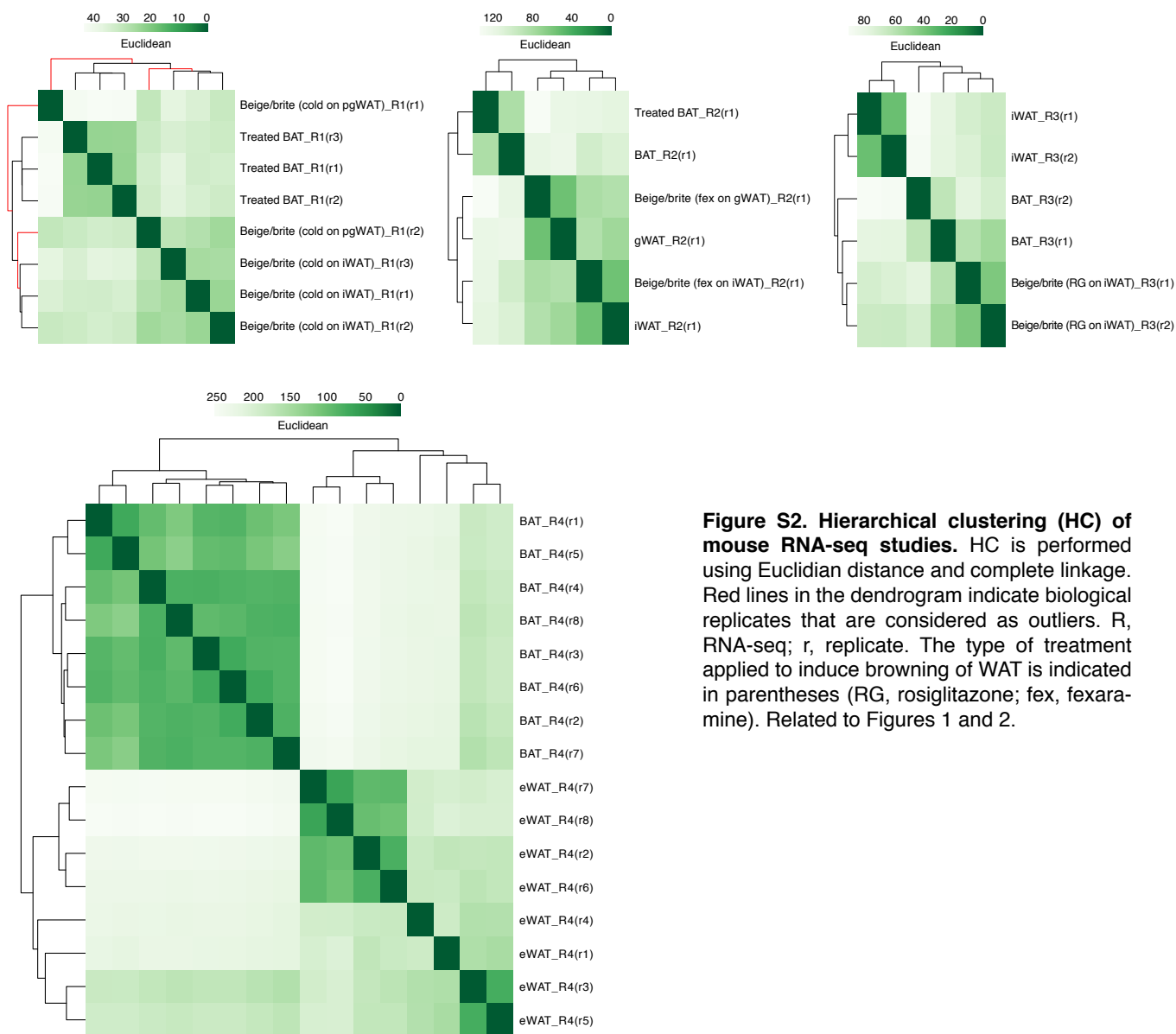


Figure S2. Hierarchical clustering (HC) of mouse RNA-seq studies. HC is performed using Euclidian distance and complete linkage. Red lines in the dendrogram indicate biological replicates that are considered as outliers. R, RNA-seq; r, replicate. The type of treatment applied to induce browning of WAT is indicated in parentheses (RG, rosiglitazone; fex, fexaramine). Related to Figures 1 and 2.

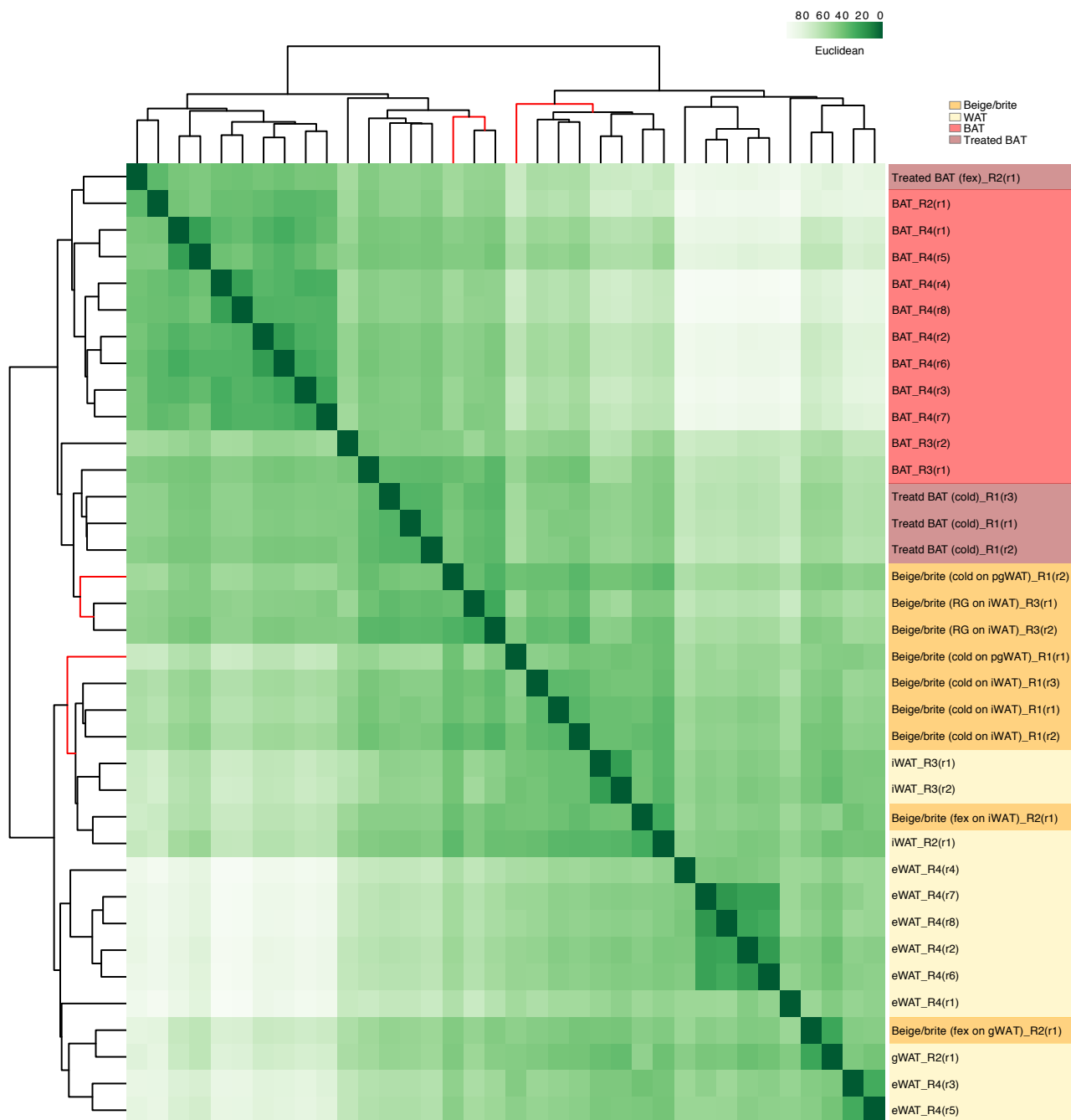


Figure S4. Hierarchical clustering of mouse samples across all RNA-seq-based studies. Euclidean distance is used for sample correlation analysis and hierarchical clustering is performed using Euclidian values and complete linkage. See **Table S1** for detailed description of each sample. Related to Figures 1 and 2.

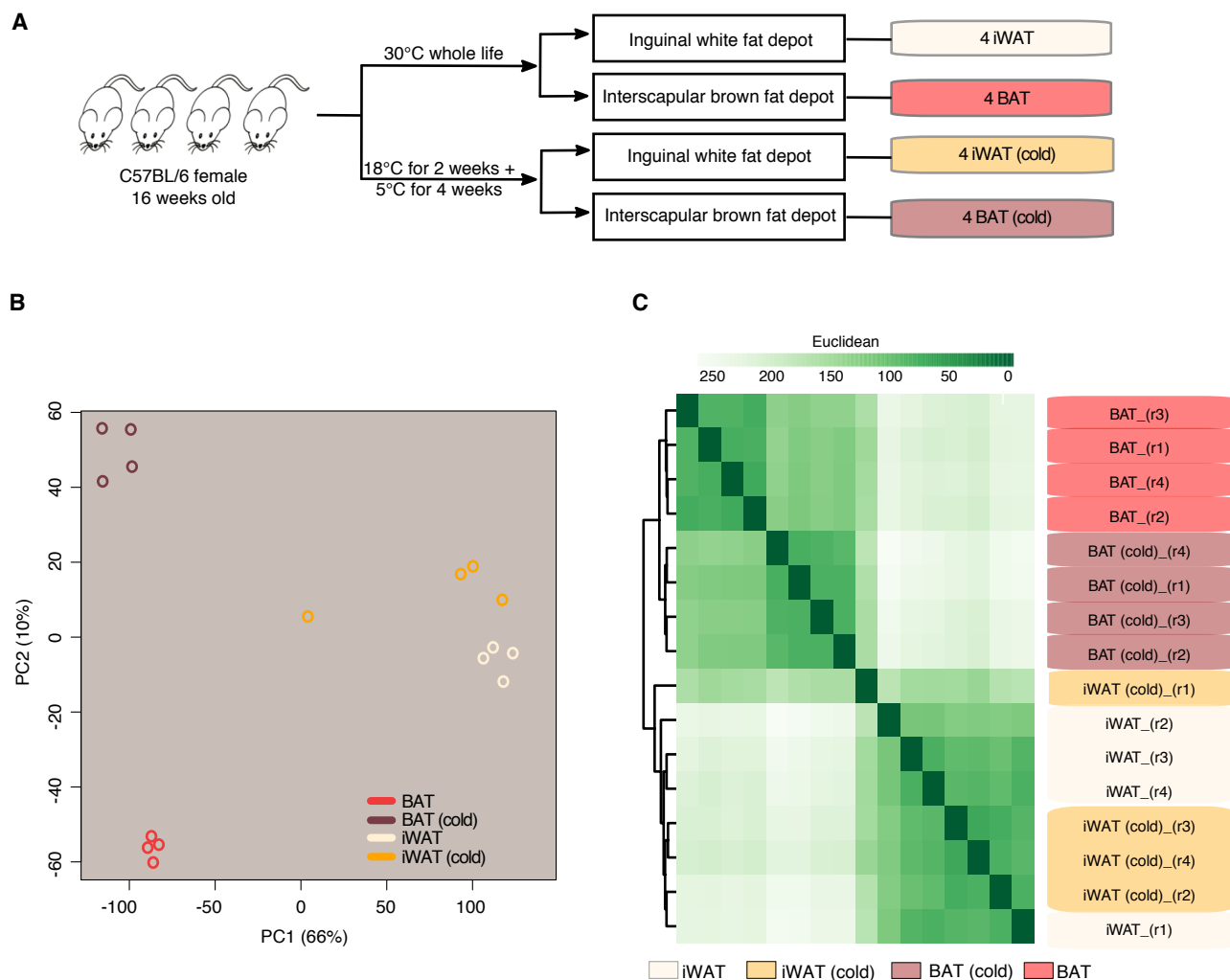


Figure S5. In-house transcriptome analysis of BAT and WAT from wild-type and cold-exposed mice. (A) Experimental design. BAT and BAT (cold), interscapular brown adipose tissue from mice kept at either 30°C or in cold ($n \geq 4$), respectively; iWAT and iWAT (cold), inguinal white adipose tissue from mice kept at either 30°C or in cold ($n \geq 4$), respectively. (B) Principle component analysis of normalized gene expression data for all biological replicates. (C) Hierarchical clustering of all samples based on gene expression data. Euclidean distance is used for pairwise distance matrix and hierarchical clustering is performed with Euclidean distance and complete linkage. Related to Figure 3.

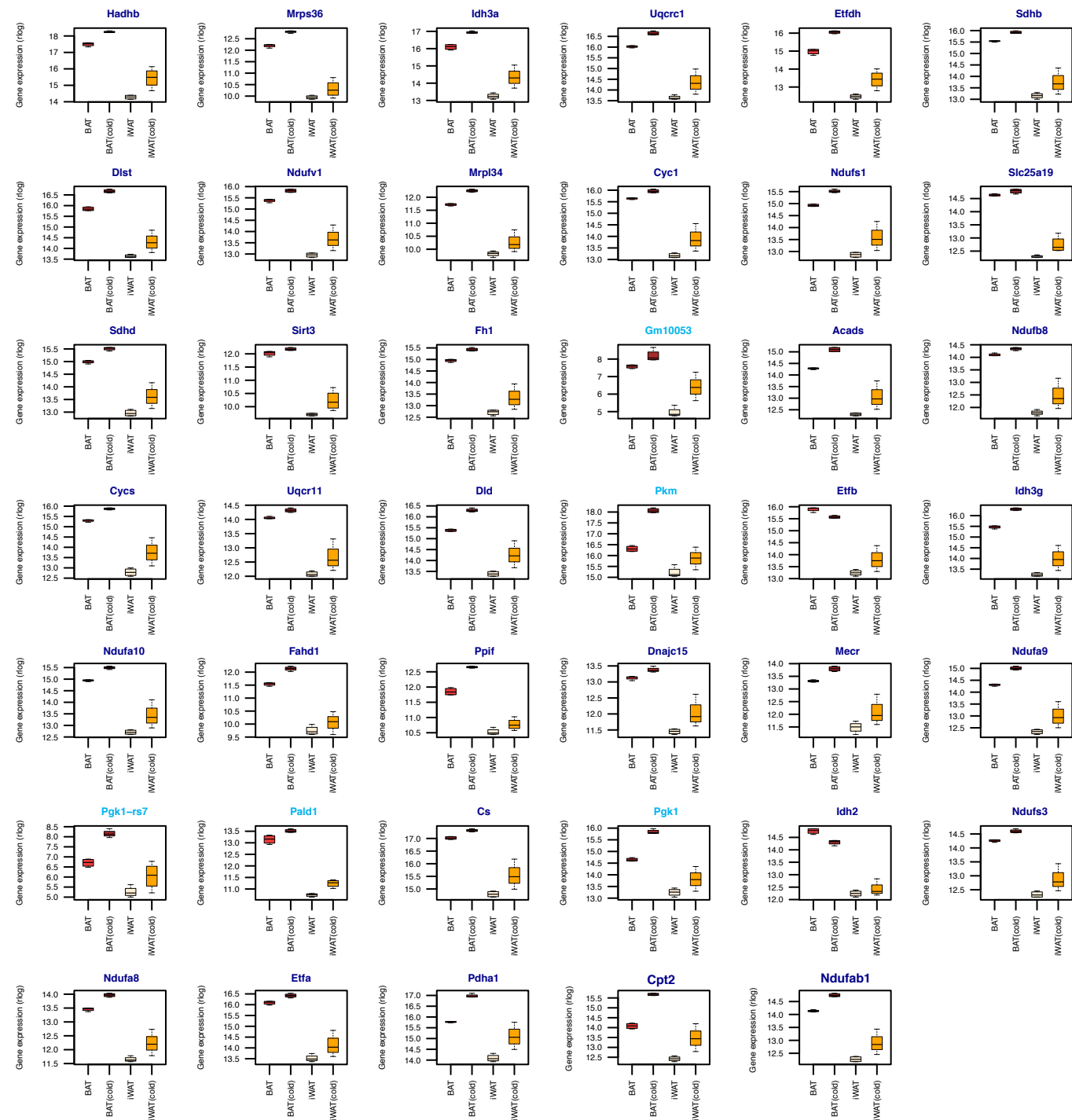


Figure S6. Experimental validation of BAT and WAT marker genes.

Gene names in blue and magenta indicate mitochondria and non-mitochondria localized markers, respectively. BAT and BAT (cold), interscapular brown adipose tissue from mice kept at either 30°C or in cold ($n \geq 4$), respectively; iWAT and iWAT (cold), inguinal white adipose tissue from mice kept at either 30°C or in cold ($n \geq 4$), respectively. Related to Figure 3.

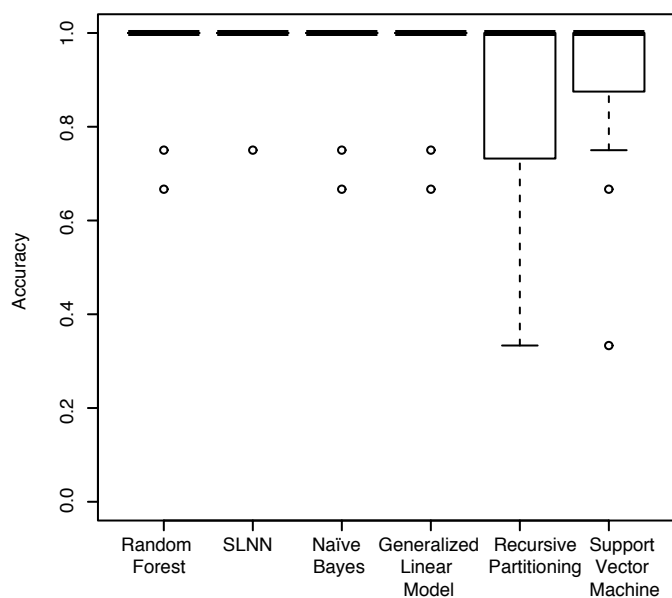
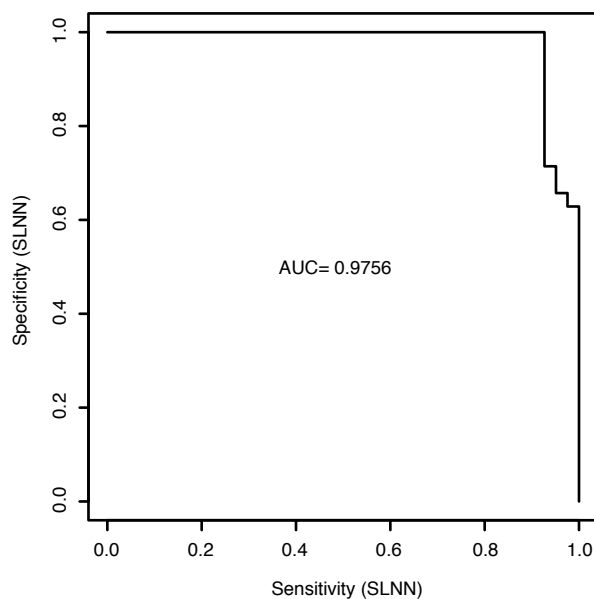
A**B**

Figure S7. Systematic comparison of the performance of machine learning algorithms for the prediction of browning capacity. (A) Accuracy of six machine learning algorithms (random forest, SLNN, naïve bayes, generalized linear model, recursive partitioning, support vector machine), trained using BAT and WAT-specific microarray and RNA-seq datasets from studies M1, M2, M4, M5, M6, M7, M12 and R4, in classifying BAT and WAT samples from an independent set of studies (M3, M8, M9, M10, M11, M13, R1, R2, R3). (B) Classification accuracy of SLNN. The accuracy is calculated as: $(TP+TN)/\text{total samples}$. A sample is a true positive if BAT was predicted with a probability > 0.5 . Related to Figure 4.

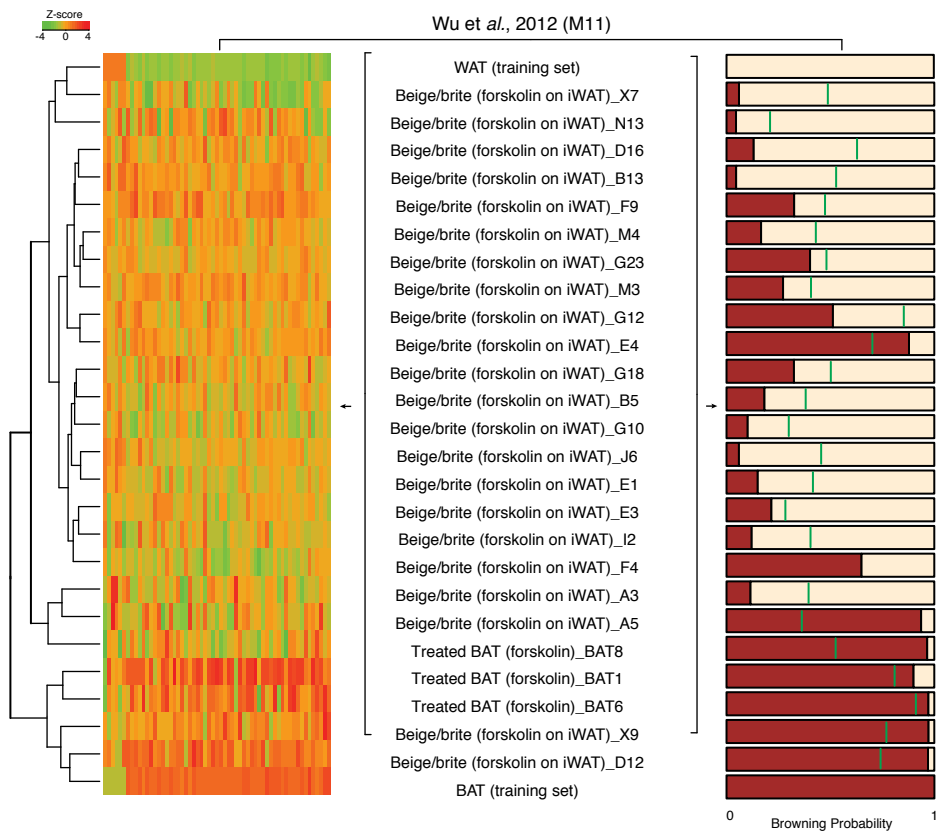


Figure S8. Prediction of browning capacity for study M11. Related to Figure 4.

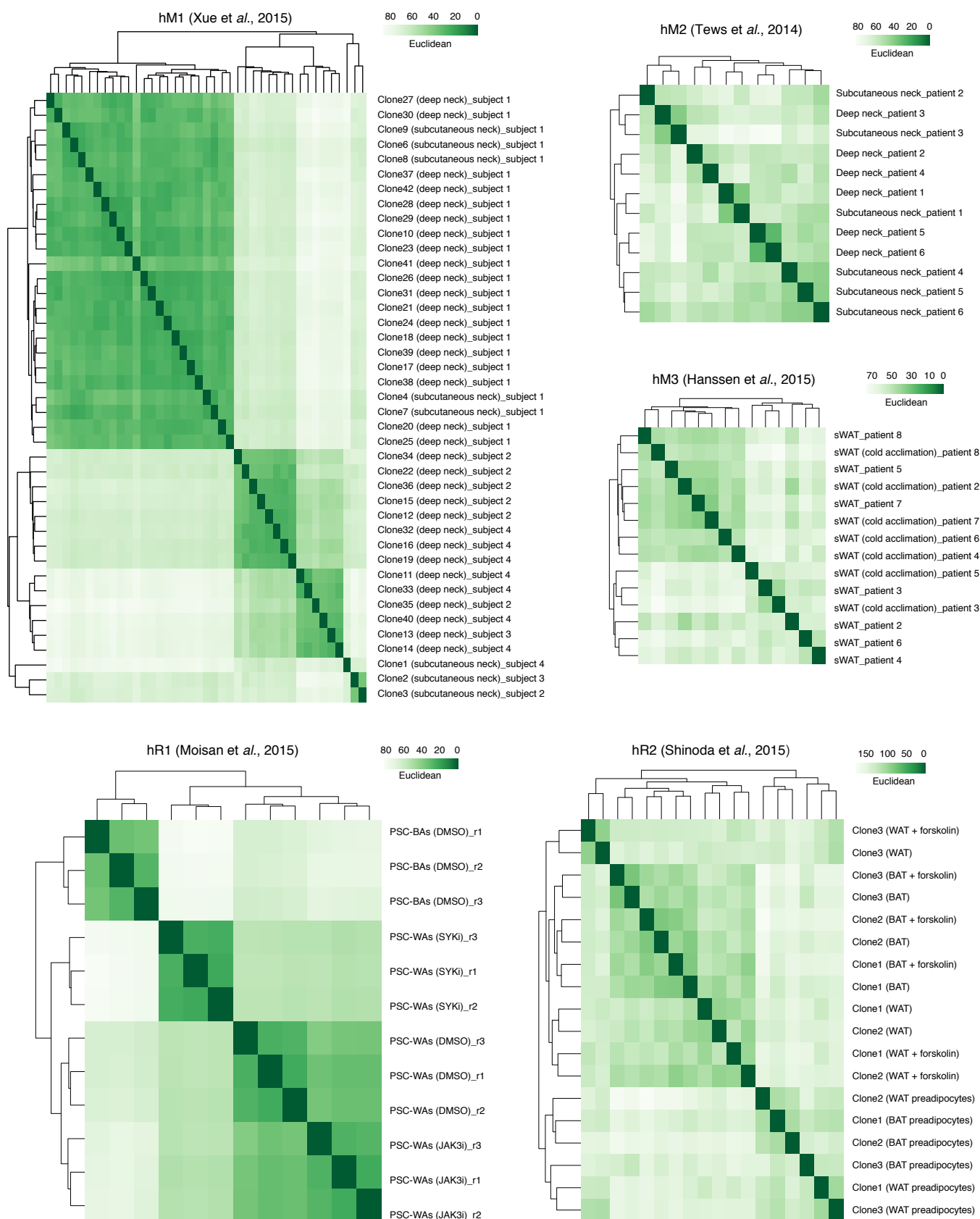


Figure S9. Hierarchical clustering (HC) of samples within each human microarray and RNA-seq study. HC is performed using Euclidian distance and complete linkage. hM, microarray on human samples; hR, RNA-seq on human samples; r, replicate. Related to Figure 5.

Supplementary Table 1. Mouse and human adipose tissue-centered gene expression atlas. WAT, white adipose tissue; IWAT, inguinal white adipose tissue; gWAT, gonadal white adipose tissue; eWAT, epididymal white adipose tissue; sWAT, subcutaneous white adipose tissue; mWAT, mesenteric white adipose tissue; pWAT, perivascular white adipose tissue; BAT, brown adipose tissue; (RG), rosiglitazone; (RF), roscovitine; fex, fexofenadine; CL, CL316.243; DID, diet-induced obesity; N/A, not available; M, microarrays; R, RNA-seq; r, biological replicate; hM, Human Microarray; hR, human RNA-Seq; SVF, stromal vascular fraction; PSC, pluripotent stem cells; BAs, brown adipocytes; WAs, white adipocytes; MRCs, mesenchymal progenitor cells. Related to Figures 1-6.

	Dataset ID	Pubmed ID	Database ID	Sample ID	Sample type	Age	Sample origin	Tissue type	Treatment	Annotation
M1	BAT_M1(y1)	15075390	GSE10246	GSM258611	Tissue	8-10 weeks	C57BL6, male	N/A	None	BAT
M1	BAT_M1(y2)	15075390	GSE10246	GSM258612	Tissue	8-10 weeks	C57BL6, male	N/A	None	BAT
M1	WAT_M1(y1)	15075390	GSE10246	GSM258613	Tissue	8-10 weeks	C57BL6, male	N/A	None	WAT
M1	WAT_M1(y2)	15075390	GSE10246	GSM258614	Tissue	8-10 weeks	C57BL6, male	N/A	None	WAT
M2	BAT_M2(y1)	20679227	GSE19757	GSM483479	Tissue	N/A	N/A	Interscapular brown adipose tissue	None	BAT
M2	BAT_M2(y2)	20679227	GSE19757	GSM493480	Tissue	N/A	N/A	Interscapular brown adipose tissue	None	BAT
M2	gWAT_M2(y1)	20679227	GSE19757	GSM493477	Tissue	N/A	N/A	Gonadal white adipose tissue	None	WAT
M2	gWAT_M2(y2)	20679227	GSE19757	GSM493478	Tissue	N/A	N/A	Gonadal white adipose tissue	None	WAT
M3	WAT_M3(y1)	22405074	GSE35011	GSM806020	Primary adipocytes	N/A	C57BL6, male	Inguinal white adipose tissue	None	WAT
M3	WAT_M3(y2)	22405074	GSE35011	GSM806021	Primary adipocytes	N/A	C57BL6, male	Inguinal white adipose tissue	None	WAT
M3	Beige/brite (IG on WAT_M3(y1))	22405074	GSE35011	GSM806022	Primary adipocytes	N/A	C57BL6, male	Inguinal white adipose tissue	Rosiglitazone (1µM)	Beige brite
M3	Beige/brite (IG on WAT_M3(y2))	22405074	GSE35011	GSM806023	Primary adipocytes	N/A	C57BL6, male	Inguinal white adipose tissue	Rosiglitazone (1µM)	Beige brite
M4	BAT_M4(y1)	21035761	GSE20165	GSM506030	Tissue	20 weeks	SV129, male	Interscapular brown adipose tissue	None	BAT
M4	BAT_M4(y2)	21035761	GSE20165	GSM506031	Tissue	20 weeks	SV129, male	Interscapular brown adipose tissue	None	BAT
M4	BAT_M4(y3)	21035761	GSE20165	GSM506032	Tissue	20 weeks	SV129, male	Interscapular brown adipose tissue	None	BAT
M4	eWAT_M4(y1)	21035761	GSE20165	GSM506024	Tissue	20 weeks	SV129, male	Epидidymal white adipose tissue	None	WAT
M4	eWAT_M4(y2)	21035761	GSE20165	GSM506025	Tissue	20 weeks	SV129, male	Epидidymal white adipose tissue	None	WAT
M4	eWAT_M4(y3)	21035761	GSE20165	GSM506026	Tissue	20 weeks	SV129, male	Epидidymal white adipose tissue	None	WAT
M5	BAT_M5(y1)	17618855	GSE8044	GSM198456	Tissue	10-12 weeks	C57BL6, male	Interscapular brown adipose tissue	None	BAT
M5	BAT_M5(y2)	17618855	GSE8044	GSM198457	Tissue	10-12 weeks	C57BL6, male	Interscapular brown adipose tissue	None	BAT
M5	BAT_M5(y3)	17618855	GSE8044	GSM198458	Tissue	10-12 weeks	C57BL6, male	Interscapular brown adipose tissue	None	BAT
M5	eWAT_M5(y1)	17618855	GSE8044	GSM198496	Tissue	10-12 weeks	C57BL6, male	Epидidymal white adipose tissue	None	WAT
M5	eWAT_M5(y2)	17618855	GSE8044	GSM198523	Tissue	10-12 weeks	C57BL6, male	Epидidymal white adipose tissue	None	WAT
M5	eWAT_M5(y3)	17618855	GSE8044	GSM198545	Tissue	10-12 weeks	C57BL6, male	Epидidymal white adipose tissue	None	WAT
M6	BAT_M6(y1)	26010905	GSE87389	GSM1646139	Tissue	N/A	LACA, male	Interscapular brown adipose tissue	None	BAT
M6	BAT_M6(y2)	26010905	GSE87389	GSM1646141	Tissue	N/A	LACA, male	Interscapular brown adipose tissue	None	BAT
M6	BAT_M6(y3)	26010905	GSE87389	GSM1646143	Tissue	N/A	LACA, male	Interscapular brown adipose tissue	None	BAT
M6	BAT_M6(y4)	26010905	GSE87389	GSM1646145	Tissue	N/A	LACA, male	Interscapular brown adipose tissue	None	BAT
M6	sWAT_M6(y1)	26010905	GSE87389	GSM1646131	Tissue	N/A	LACA, male	Subcutaneous white adipose tissue	None	WAT
M6	sWAT_M6(y2)	26010905	GSE87389	GSM1646133	Tissue	N/A	LACA, male	Subcutaneous white adipose tissue	None	WAT
M6	sWAT_M6(y3)	26010905	GSE87389	GSM1646135	Tissue	N/A	LACA, male	Subcutaneous white adipose tissue	None	WAT
M6	sWAT_M6(y4)	26010905	GSE87389	GSM1646137	Tissue	N/A	LACA, male	Subcutaneous white adipose tissue	None	WAT
M7	BAT_M7(y1)	17360536	GSE7032	GSM162537	Primary adipocytes	3-4 weeks	NMRI	Interscapular brown adipose tissue	None	BAT
M7	BAT_M7(y2)	17360536	GSE7032	GSM162538	Primary adipocytes	3-4 weeks	NMRI	Interscapular brown adipose tissue	None	BAT
M7	BAT_M7(y3)	17360536	GSE7032	GSM162539	Primary adipocytes	3-4 weeks	NMRI	Interscapular brown adipose tissue	None	BAT
M7	BAT_M7(y4)	17360536	GSE7032	GSM162540	Primary adipocytes	3-4 weeks	NMRI	Interscapular brown adipose tissue	None	BAT
M7	BAT_M7(y5)	17360536	GSE7032	GSM162541	Primary adipocytes	3-4 weeks	NMRI	Interscapular brown adipose tissue	None	BAT
M7	eWAT_M7(y1)	17360536	GSE7032	GSM162550	Primary adipocytes	3-4 weeks	NMRI	Epидidymal white adipose tissue	None	WAT
M7	eWAT_M7(y2)	17360536	GSE7032	GSM162551	Primary adipocytes	3-4 weeks	NMRI	Epидidymal white adipose tissue	None	WAT
M7	eWAT_M7(y3)	17360536	GSE7032	GSM162552	Primary adipocytes	3-4 weeks	NMRI	Epидidymal white adipose tissue	None	WAT
M7	eWAT_M7(y4)	17360536	GSE7032	GSM162553	Primary adipocytes	3-4 weeks	NMRI	Epидidymal white adipose tissue	None	WAT
M7	eWAT_M7(y5)	17360536	GSE7032	GSM162554	Primary adipocytes	3-4 weeks	NMRI	Epидidymal white adipose tissue	None	WAT
M7	eWAT_M7(y6)	17360536	GSE7032	GSM162555	Primary adipocytes	3-4 weeks	NMRI	Epидidymal white adipose tissue	None	WAT
M8	WAT_M8(y1)	19117550	GSE13432	GSM338989	Tissue	5 weeks	C57BL6, male	Inguinal white adipose tissue	30 °C (5 weeks)	WAT
M8	WAT_M8(y2)	19117550	GSE13432	GSM338990	Tissue	5 weeks	C57BL6, male	Inguinal white adipose tissue	30 °C (5 weeks)	WAT
M8	WAT_M8(y3)	19117550	GSE13432	GSM338991	Tissue	5 weeks	C57BL6, male	Inguinal white adipose tissue	30 °C (5 weeks)	WAT
M8	WAT_M8(y4)	19117550	GSE13432	GSM338983	Tissue	5 weeks	C57BL6, male	Inguinal white adipose tissue	30 °C (1 week)	WAT
M8	WAT_M8(y5)	19117550	GSE13432	GSM338984	Tissue	5 weeks	C57BL6, male	Inguinal white adipose tissue	30 °C (1 week)	WAT
M8	WAT_M8(y6)	19117550	GSE13432	GSM338985	Tissue	5 weeks	C57BL6, male	Inguinal white adipose tissue	30 °C (1 week)	WAT
M8	Beige/brite (cold on WAT_M8(y1))	19117550	GSE13432	GSM338992	Tissue	5 weeks	C57BL6, male	Inguinal white adipose tissue	4 °C (5 weeks)	Beige/brite
M8	Beige/brite (cold on WAT_M8(y2))	19117550	GSE13432	GSM338993	Tissue	5 weeks	C57BL6, male	Inguinal white adipose tissue	4 °C (5 weeks)	Beige/brite
M8	Beige/brite (cold on WAT_M8(y3))	19117550	GSE13432	GSM338994	Tissue	5 weeks	C57BL6, male	Inguinal white adipose tissue	4 °C (5 weeks)	Beige/brite
M8	Beige/brite (cold on WAT_M8(y4))	19117550	GSE13432	GSM338986	Tissue	5 weeks	C57BL6, male	Inguinal white adipose tissue	4 °C (1 week)	Beige/brite
M8	Beige/brite (cold on WAT_M8(y5))	19117550	GSE13432	GSM338987	Tissue	5 weeks	C57BL6, male	Inguinal white adipose tissue	4 °C (1 week)	Beige/brite
M8	Beige/brite (cold on WAT_M8(y6))	19117550	GSE13432	GSM338988	Tissue	5 weeks	C57BL6, male	Inguinal white adipose tissue	4 °C (1 week)	Beige/brite
M9	BAT_M9(y1)	21765057	GSE28440	GSM703077	Tissue	20 weeks	C57BL6, male	Interscapular brown adipose tissue	None	BAT
M9	BAT_M9(y2)	21765057	GSE28440	GSM703078	Tissue	20 weeks	C57BL6, male	Interscapular brown adipose tissue	None	BAT
M9	BAT_M9(y3)	21765057	GSE28440	GSM703079	Tissue	20 weeks	C57BL6, male	Interscapular brown adipose tissue	None	BAT
M9	eWAT_M9(y1)	21765057	GSE28440	GSM703086	Tissue	20 weeks	C57BL6, male	Epидidymal white adipose tissue	None	WAT
M9	eWAT_M9(y2)	21765057	GSE28440	GSM703087	Tissue	20 weeks	C57BL6, male	Epидidymal white adipose tissue	None	WAT
M9	eWAT_M9(y3)	21765057	GSE28440	GSM703088	Tissue	20 weeks	C57BL6, male	Epидidymal white adipose tissue	None	WAT
M9	pWAT_M9(y1)	21765057	GSE28440	GSM703080	Tissue	20 weeks	C57BL6, male	Perivascular white adipose tissue	None	WAT
M9	pWAT_M9(y2)	21765057	GSE28440	GSM703081	Tissue	20 weeks	C57BL6, male	Perivascular white adipose tissue	None	WAT
M9	pWAT_M9(y3)	21765057	GSE28440	GSM703082	Tissue	20 weeks	C57BL6, male	Perivascular white adipose tissue	None	WAT
M9	WAT_M9(y1)	21765057	GSE28440	GSM703083	Tissue	20 weeks	C57BL6, male	inguinal white adipose tissue	None	WAT
M9	WAT_M9(y2)	21765057	GSE28440	GSM703084	Tissue	20 weeks	C57BL6, male	inguinal white adipose tissue	None	WAT
M9	WAT_M9(y3)	21765057	GSE28440	GSM703085	Tissue	20 weeks	C57BL6, male	inguinal white adipose tissue	None	WAT
M10	BAT_M10(y1)	24549398	GSE51080	GSM1237806	Tissue	10 weeks	SV129, female	Interscapular brown adipose tissue	28 °C (10 days)	BAT
M10	BAT_M10(y2)	24549398	GSE51080	GSM1237794	Tissue	10 weeks	SV129, female	Interscapular brown adipose tissue	28 °C (10 days)	BAT
M10	BAT_M10(y3)	24549398	GSE51080	GSM1237795	Tissue	10 weeks	SV129, female	Interscapular brown adipose tissue	28 °C (10 days)	BAT
M10	Treated BAT (cold, M10(y1))	24549398	GSE51080	GSM1237792	Tissue	10 weeks	SV129, female	Interscapular brown adipose tissue	6 °C (10 days)	Treated BAT
M10	Treated BAT (cold, M10(y2))	24549398	GSE51080	GSM1237800	Tissue	10 weeks	SV129, female	Interscapular brown adipose tissue	6 °C (10 days)	Treated BAT
M10	Treated BAT (cold, M10(y3))	24549398	GSE51080	GSM1237803	Tissue	10 weeks	SV129, female	Interscapular brown adipose tissue	6 °C (10 days)	Treated BAT
M10	sWAT_M10(y1)	24549398	GSE51080	GSM1237797	Tissue	10 weeks	SV129, female	Subcutaneous white adipose tissue	28 °C (10 days)	WAT
M10	sWAT_M10(y2)	24549398	GSE51080	GSM1237798	Tissue	10 weeks	SV129, female	Subcutaneous white adipose tissue	28 °C (10 days)	WAT
M10	sWAT_M10(y3)	24549398	GSE51080	GSM1237793	Tissue	10 weeks	SV129, female	Subcutaneous white adipose tissue	28 °C (10 days)	WAT
M10	Beige/brite (cold on sWAT_M10(y1))	24549398	GSE51080	GSM1237790	Tissue	10 weeks	SV129, female	Subcutaneous white adipose tissue	6 °C (10 days)	Beige/brite
M10	Beige/brite (cold on sWAT_M10(y2))	24549398	GSE51080	GSM1237796	Tissue	10 weeks	SV129, female	Subcutaneous white adipose tissue	6 °C (10 days)	Beige/brite
M10	Beige/brite (cold on sWAT_M10(y3))	24549398	GSE51080	GSM1237799	Tissue	10 weeks	SV129, female	Subcutaneous white adipose tissue	6 °C (10 days)	Beige/brite
M10	mWAT_M10(y1)	24549398	GSE51080	GSM1237801	Tissue	10 weeks	SV129, female	Mesenteric white adipose tissue	28 °C (10 days)	WAT
M10	mWAT_M10(y2)	24549398	GSE51080	GSM1237802	Tissue	10 weeks	SV129, female	Mesenteric white adipose tissue	28 °C (10 days)	WAT
M10	mWAT_M10(y3)	24549398	GSE51080	GSM1237791	Tissue	10 weeks	SV129, female	Mesenteric white adipose tissue	28 °C (10 days)	WAT
M10	Beige/brite (cold on mWAT_M10(y1))	24549398	GSE51080	GSM1237804	Tissue	10 weeks	SV129, female	Mesenteric white adipose tissue	6 °C (10 days)	Beige/brite
M10	Beige/brite (cold on mWAT_M10(y2))	24549398	GSE51080	GSM1237805	Tissue	10 weeks	SV129, female	Mesenteric white adipose tissue	6 °C (10 days)	Beige/brite
M10	Beige/brite (cold on mWAT_M10(y3))	24549398	GSE51080	GSM1237807	Tissue	10 weeks	SV129, female	Mesenteric white adipose tissue	6 °C (10 days)	Beige/brite

[illegible]

R2	BAT_R2(1)	2559344	SRA188644	SRR1625955	Tissue	14 weeks	C57BL6 DIO	Interscapular brown adipose tissue	Vehicle		BAT
R2	Treated BAT (lex_R2(1)	2559344	SRA188644	SRR1602556	Tissue	14 weeks	C57BL6 DIO	Interscapular brown adipose tissue	Vehicle		Treated BAT
R2	/iWAT_R2(1)	2559344	SRA188644	SRR1597458	Tissue	14 weeks	C57BL6 DIO	Inguinal white adipose tissue	Flex		WAT
R2	Beige/brite (flex on iWAT)_R2(1)	2559344	SRA188644	SRR1597454	Tissue	14 weeks	C57BL6 DIO	Inguinal white adipose tissue	Flex		Beige/brite
R2	gWAT_R2(1)	2559344	SRA188644	SRR1596699	Tissue	14 weeks	C57BL6 DIO	Gonadal white adipose tissue	Vehicle		WAT
R2	Beige/brite (flex on gWAT)_R2(1)	2559344	SRA188644	SRR1597452	Tissue	14 weeks	C57BL6 DIO	Gonadal white adipose tissue	Flex		Beige/brite
R3	BAT_R3(1)	2316672	E-MTAB-2624	ERS472803	Primary adipocytes	N/A	N/A	Interscapular brown adipose tissue	None		BAT
R3	BAT_R3(2)	2316672	E-MTAB-2624	ERS472808	Primary adipocytes	N/A	N/A	Interscapular brown adipose tissue	None		BAT
R3	/iWAT_R3(1)	2316672	E-MTAB-2624	ERS472804	Primary adipocytes	N/A	N/A	Inguinal white adipose tissue	None		WAT
R3	/iWAT_R3(2)	2316672	E-MTAB-2624	ERS472806	Primary adipocytes	N/A	N/A	Inguinal white adipose tissue	None		WAT
R3	Beige/brite (RG on iWAT)_R3(1)	2316672	E-MTAB-2624	ERS472807	Primary adipocytes	N/A	N/A	Inguinal white adipose tissue	Rosiglitazone (1µM)		Beige/brite
R3	Beige/brite (RG on iWAT)_R3(2)	2316672	E-MTAB-2624	ERS472805	Primary adipocytes	N/A	N/A	Inguinal white adipose tissue	Rosiglitazone (1µM)		Beige/brite
R4	BAT_R4(1)	2534387	GSE54651	GSM1321302	Tissue	6 weeks	C57BL6, male	Interscapular brown adipose tissue	None		BAT
R4	BAT_R4(2)	2534387	GSE54651	GSM1321303	Tissue	6 weeks	C57BL6, male	Interscapular brown adipose tissue	None		BAT
R4	BAT_R4(3)	2534387	GSE54651	GSM1321304	Tissue	6 weeks	C57BL6, male	Interscapular brown adipose tissue	None		BAT
R4	BAT_R4(4)	2534387	GSE54651	GSM1321305	Tissue	6 weeks	C57BL6, male	Interscapular brown adipose tissue	None		BAT
R4	BAT_R4(5)	2534387	GSE54651	GSM1321306	Tissue	6 weeks	C57BL6, male	Interscapular brown adipose tissue	None		BAT
R4	BAT_R4(6)	2534387	GSE54651	GSM1321307	Tissue	6 weeks	C57BL6, male	Interscapular brown adipose tissue	None		BAT
R4	BAT_R4(7)	2534387	GSE54651	GSM1321308	Tissue	6 weeks	C57BL6, male	Interscapular brown adipose tissue	None		BAT
R4	BAT_R4(8)	2534387	GSE54651	GSM1321309	Tissue	6 weeks	C57BL6, male	Interscapular brown adipose tissue	None		BAT
R4	eWAT_R4(1)	2534387	GSE54651	GSM1321366	Tissue	6 weeks	C57BL6, male	Epididymal white adipose tissue	None		WAT
R4	eWAT_R4(2)	2534387	GSE54651	GSM1321367	Tissue	6 weeks	C57BL6, male	Epididymal white adipose tissue	None		WAT
R4	eWAT_R4(3)	2534387	GSE54651	GSM1321368	Tissue	6 weeks	C57BL6, male	Epididymal white adipose tissue	None		WAT
R4	eWAT_R4(4)	2534387	GSE54651	GSM1321369	Tissue	6 weeks	C57BL6, male	Epididymal white adipose tissue	None		WAT
R4	eWAT_R4(5)	2534387	GSE54651	GSM1321370	Tissue	6 weeks	C57BL6, male	Epididymal white adipose tissue	None		WAT
R4	eWAT_R4(6)	2534387	GSE54651	GSM1321371	Tissue	6 weeks	C57BL6, male	Epididymal white adipose tissue	None		WAT
R4	eWAT_R4(7)	2534387	GSE54651	GSM1321372	Tissue	6 weeks	C57BL6, male	Epididymal white adipose tissue	None		WAT
R4	eWAT_R4(8)	2534387	GSE54651	GSM1321373	Tissue	6 weeks	C57BL6, male	Epididymal white adipose tissue	None		WAT
NM1	C1one1 (subcutaneous neck)_subject 4	2607636	GSE85854	GSM1674867	SVF cells from subcutaneous and subclavicular neck	N/A	Subject 4	Immortalized human clonal preadipocytes	Immortalization, culture, differentiation		N/A
NM1	C1one2 (subcutaneous neck)_subject 3	2607636	GSE85854	GSM1674868	SVF cells from subcutaneous and subclavicular neck	N/A	Subject 3	Immortalized human clonal preadipocytes	Immortalization, culture, differentiation		N/A
NM1	C1one3 (subcutaneous neck)_subject 2	2607636	GSE85854	GSM1674869	SVF cells from subcutaneous and subclavicular neck	N/A	Subject 2	Immortalized human clonal preadipocytes	Immortalization, culture, differentiation		N/A
NM1	C1one4 (subcutaneous neck)_subject 1	2607636	GSE85854	GSM1674870	SVF cells from subcutaneous and subclavicular neck	N/A	Subject 1	Immortalized human clonal preadipocytes	Immortalization, culture, differentiation		N/A
NM1	C1one5 (subcutaneous neck)_subject 1	2607636	GSE85854	GSM1674871	SVF cells from subcutaneous and subclavicular neck	N/A	Subject 1	Immortalized human clonal preadipocytes	Immortalization, culture, differentiation		N/A
NM1	C1one7 (subcutaneous neck)_subject 1	2607636	GSE85854	GSM1674872	SVF cells from subcutaneous and subclavicular neck	N/A	Subject 1	Immortalized human clonal preadipocytes	Immortalization, culture, differentiation		N/A
NM1	C1one6 (subcutaneous neck)_subject 1	2607636	GSE85854	GSM1674873	SVF cells from subcutaneous and subclavicular neck	N/A	Subject 1	Immortalized human clonal preadipocytes	Immortalization, culture, differentiation		N/A
NM1	C1one9 (subcutaneous neck)_subject 1	2607636	GSE85854	GSM1674874	SVF cells from subcutaneous and subclavicular neck	N/A	Subject 1	Immortalized human clonal preadipocytes	Immortalization, culture, differentiation		N/A
NM1	C1one10 (deep neck)_subject 1	2607636	GSE85854	GSM1674875	SVF cells from deep neck	N/A	Subject 1	Immortalized human clonal preadipocytes	Immortalization, culture, differentiation		N/A
NM1	C1one11 (deep neck)_subject 4	2607636	GSE85854	GSM1674876	SVF cells from deep neck	N/A	Subject 4	Immortalized human clonal preadipocytes	Immortalization, culture, differentiation		N/A
NM1	C1one12 (deep neck)_subject 2	2607636	GSE85854	GSM1674877	SVF cells from deep neck	N/A	Subject 2	Immortalized human clonal preadipocytes	Immortalization, culture, differentiation		N/A
NM1	C1one13 (deep neck)_subject 3	2607636	GSE85854	GSM1674878	SVF cells from deep neck	N/A	Subject 3	Immortalized human clonal preadipocytes	Immortalization, culture, differentiation		N/A
NM1	C1one14 (deep neck)_subject 4	2607636	GSE85854	GSM1674879	SVF cells from deep neck	N/A	Subject 4	Immortalized human clonal preadipocytes	Immortalization, culture, differentiation		N/A
NM1	C1one15 (deep neck)_subject 2	2607636	GSE85854	GSM1674880	SVF cells from deep neck	N/A	Subject 2	Immortalized human clonal preadipocytes	Immortalization, culture, differentiation		N/A
NM1	C1one16 (deep neck)_subject 4	2607636	GSE85854	GSM1674881	SVF cells from deep neck	N/A	Subject 4	Immortalized human clonal preadipocytes	Immortalization, culture, differentiation		N/A
NM1	C1one17 (deep neck)_subject 1	2607636	GSE85854	GSM1674882	SVF cells from deep neck	N/A	Subject 1	Immortalized human clonal preadipocytes	Immortalization, culture, differentiation		N/A
NM1	C1one18 (deep neck)_subject 1	2607636	GSE85854	GSM1674883	SVF cells from deep neck	N/A	Subject 1	Immortalized human clonal preadipocytes	Immortalization, culture, differentiation		N/A
NM1	C1one19 (deep neck)_subject 4	2607636	GSE85854	GSM1674884	SVF cells from deep neck	N/A	Subject 4	Immortalized human clonal preadipocytes	Immortalization, culture, differentiation		N/A
NM1	C1one20 (deep neck)_subject 1	2607636	GSE85854	GSM1674885	SVF cells from deep neck	N/A	Subject 1	Immortalized human clonal preadipocytes	Immortalization, culture, differentiation		N/A
NM1	C1one21 (deep neck)_subject 1	2607636	GSE85854	GSM1674886	SVF cells from deep neck	N/A	Subject 1	Immortalized human clonal preadipocytes	Immortalization, culture, differentiation		N/A
NM1	C1one22 (deep neck)_subject 2	2607636	GSE85854	GSM1674887	SVF cells from deep neck	N/A	Subject 2	Immortalized human clonal preadipocytes	Immortalization, culture, differentiation		N/A
NM1	C1one23 (deep neck)_subject 1	2607636	GSE85854	GSM1674888	SVF cells from deep neck	N/A	Subject 1	Immortalized human clonal preadipocytes	Immortalization, culture, differentiation		N/A
NM1	C1one24 (deep neck)_subject 1	2607636	GSE85854	GSM1674889	SVF cells from deep neck	N/A	Subject 1	Immortalized human clonal preadipocytes	Immortalization, culture, differentiation		N/A
NM1	C1one25 (deep neck)_subject 1	2607636	GSE85854	GSM1674890	SVF cells from deep neck	N/A	Subject 1	Immortalized human clonal preadipocytes	Immortalization, culture, differentiation		N/A
NM1	C1one26 (deep neck)_subject 1	2607636	GSE85854	GSM1674891	SVF cells from deep neck	N/A	Subject 1	Immortalized human clonal preadipocytes	Immortalization, culture, differentiation		N/A
NM1	C1one27 (deep neck)_subject 1	2607636	GSE85854	GSM1674892	SVF cells from deep neck	N/A	Subject 1	Immortalized human clonal preadipocytes	Immortalization, culture, differentiation		N/A
NM1	C1one28 (deep neck)_subject 1	2607636	GSE85854	GSM1674893	SVF cells from deep neck	N/A	Subject 1	Immortalized human clonal preadipocytes	Immortalization, culture, differentiation		N/A
NM1	C1one29 (deep neck)_subject 1	2607636	GSE85854	GSM1674894	SVF cells from deep neck	N/A	Subject 1	Immortalized human clonal preadipocytes	Immortalization, culture, differentiation		N/A
NM1	C1one30 (deep neck)_subject 1	2607636	GSE85854	GSM1674895	SVF cells from deep neck	N/A	Subject 1	Immortalized human clonal preadipocytes	Immortalization, culture, differentiation		N/A
NM1	C1one31 (deep neck)_subject 1	2607636	GSE85854	GSM1674896	SVF cells from deep neck	N/A	Subject 1	Immortalized human clonal preadipocytes	Immortalization, culture, differentiation		N/A
NM1	C1one32 (deep neck)_subject 4	2607636	GSE85854	GSM1674897	SVF cells from deep neck	N/A	Subject 4	Immortalized human clonal preadipocytes	Immortalization, culture, differentiation		N/A
NM1	C1one33 (deep neck)_subject 4	2607636	GSE85854	GSM1674898	SVF cells from deep neck	N/A	Subject 4	Immortalized human clonal preadipocytes	Immortalization, culture, differentiation		N/A
NM1	C1one34 (deep neck)_subject 2	2607636	GSE85854	GSM1674899	SVF cells from deep neck	N/A	Subject 2	Immortalized human clonal preadipocytes	Immortalization, culture, differentiation		N/A
NM1	C1one35 (deep neck)_subject 2	2607636	GSE85854	GSM1674900	SVF cells from deep neck	N/A	Subject 2	Immortalized human clonal preadipocytes	Immortalization, culture, differentiation		N/A
NM1	C1one36 (deep neck)_subject 1	2607636	GSE85854	GSM1674901	SVF cells from deep neck	N/A	Subject 1	Immortalized human clonal preadipocytes	Immortalization, culture, differentiation		N/A
NM1	C1one37 (deep neck)_subject 1	2607636	GSE85854	GSM1674902	SVF cells from deep neck	N/A	Subject 1	Immortalized human clonal preadipocytes	Immortalization, culture, differentiation		N/A
NM1	C1one38 (deep neck)_subject 1	2607636	GSE85854	GSM1674903	SVF cells from deep neck	N/A	Subject 1	Immortalized human clonal preadipocytes	Immortalization, culture, differentiation		N/A
NM1	C1one39 (deep neck)_subject 1	2607636	GSE85854	GSM1674904	SVF cells from deep neck	N/A	Subject 1	Immortalized human clonal preadipocytes	Immortalization, culture, differentiation		N/A
NM1	C1one40 (deep neck)_subject 4	2607636	GSE85854	GSM1674905	SVF cells from deep neck	N/A	Subject 4	Immortalized human clonal preadipocytes	Immortalization, culture, differentiation		N/A
NM1	C1one41 (deep neck)_subject 1	2607636	GSE85854	GSM1674906	SVF cells from deep neck	N/A	Subject 1	Immortalized human clonal preadipocytes	Immortalization, culture, differentiation		N/A
NM1	C1one42 (deep neck)_subject 1	2607636	GSE85854	GSM1674907	SVF cells from deep neck	N/A	Subject 1	Immortalized human clonal preadipocytes	Immortalization, culture, differentiation		N/A
NM2	Deep neck_patient 1	2510227	GSE54280	GSM1311783	Deep neck	N/A	Patient 1	Primary human adipocytes	None		N/A
NM2	Deep neck_patient 2	2510227	GSE54280	GSM1311785	Deep neck	N/A	Patient 2	Primary human adipocytes	None		N/A
NM2	Deep neck_patient 3	2510227	GSE54280	GSM1311787	Deep neck	N/A	Patient 3	Primary human adipocytes	None		N/A
NM2	Deep neck_patient 4	2510227	GSE54280	GSM1311789	Deep neck	N/A	Patient 4	Primary human adipocytes	None		N/A
NM2	Deep neck_patient 5	2510227	GSE54280	GSM1311791	Deep neck	N/A	Patient 5	Primary human adipocytes	None		N/A
NM2	Deep neck_patient 6	2510227	GSE54280	GSM1311793	Deep neck	N/A	Patient 6	Primary human adipocytes	None		N/A
NM2	Subcutaneous neck_patient 1	2510227	GSE54280	GSM1311784	Subcutaneous neck	N/A	Patient 1	Primary human adipocytes	None		N/A
NM2	Subcutaneous neck_patient 2	2510227	GSE54280	GSM1311786	Subcutaneous neck	N/A	Patient 2	Primary human adipocytes	None		N/A
NM2	Subcutaneous neck_patient 3	2510227	GSE54280	GSM1311788	Subcutaneous neck	N/A	Patient 3	Primary human adipocytes	None		N/A
NM2	Subcutaneous neck_patient 4	2510227	GSE54280	GSM1311790	Subcutaneous neck	N/A	Patient 4	Primary human adipocytes	None		N/A
NM2	Subcutaneous neck_patient 5	2510227	GSE54280	GSM1311792	Subcutaneous neck	N/A	Patient 5	Primary human adipocytes	None		N/A
NM2	Subcutaneous neck_patient 6	2510227	GSE54280	GSM1311794	Subcutaneous neck	N/A	Patient 6	Primary human adipocytes	None		N/A
NM3	sWAT (cold acclimation)_patient 2	2614790	GSE67297	GSM164008	Abdominal subcutaneous fat	N/A	Patient 2	Primary adipocytes from human type 2 diabetic patients	After 10 days of cold acclimation		N/A

HM3	sWAT (cold acclimation)_patient 3	26147760	GSE67297	GSM1644012	Abdominal subcutaneous fat	N/A	Patient 3	Primary adipocytes from human type 2 diabetic patients	After 10 days of cold acclimation	N/A
HM3	sWAT (cold acclimation)_patient 4	26147760	GSE67297	GSM1644016	Abdominal subcutaneous fat	N/A	Patient 4	Primary adipocytes from human type 2 diabetic patients	After 10 days of cold acclimation	N/A
HM3	sWAT (cold acclimation)_patient 5	26147760	GSE67297	GSM1644005	Abdominal subcutaneous fat	N/A	Patient 5	Primary adipocytes from human type 2 diabetic patients	After 10 days of cold acclimation	N/A
HM3	sWAT (cold acclimation)_patient 6	26147760	GSE67297	GSM1644009	Abdominal subcutaneous fat	N/A	Patient 6	Primary adipocytes from human type 2 diabetic patients	After 10 days of cold acclimation	N/A
HM3	sWAT (cold acclimation)_patient 7	26147760	GSE67297	GSM1644013	Abdominal subcutaneous fat	N/A	Patient 7	Primary adipocytes from human type 2 diabetic patients	After 10 days of cold acclimation	N/A
HM3	sWAT (cold acclimation)_patient 8	26147760	GSE67297	GSM1644017	Abdominal subcutaneous fat	N/A	Patient 8	Primary adipocytes from human type 2 diabetic patients	After 10 days of cold acclimation	N/A
HM3	sWAT_patient 2	26147760	GSE67297	GSM1644006	Abdominal subcutaneous fat	N/A	Patient 2	Primary adipocytes from human type 2 diabetic patients	Before cold acclimation	N/A
HM3	sWAT_patient 3	26147760	GSE67297	GSM1644010	Abdominal subcutaneous fat	N/A	Patient 3	Primary adipocytes from human type 2 diabetic patients	Before cold acclimation	N/A
HM3	sWAT_patient 4	26147760	GSE67297	GSM1644014	Abdominal subcutaneous fat	N/A	Patient 4	Primary adipocytes from human type 2 diabetic patients	Before cold acclimation	N/A
HM3	sWAT_patient 5	26147760	GSE67297	GSM1644004	Abdominal subcutaneous fat	N/A	Patient 5	Primary adipocytes from human type 2 diabetic patients	Before cold acclimation	N/A
HM3	sWAT_patient 6	26147760	GSE67297	GSM1644007	Abdominal subcutaneous fat	N/A	Patient 6	Primary adipocytes from human type 2 diabetic patients	Before cold acclimation	N/A
HM3	sWAT_patient 7	26147760	GSE67297	GSM1644011	Abdominal subcutaneous fat	N/A	Patient 7	Primary adipocytes from human type 2 diabetic patients	Before cold acclimation	N/A
HM3	sWAT_patient 8	26147760	GSE67297	GSM1644015	Abdominal subcutaneous fat	N/A	Patient 8	Primary adipocytes from human type 2 diabetic patients	Before cold acclimation	N/A
HR1	PSC-BAs (DMSO)_r1	25487280	SRP042186	GSM1396748	ventilated from PPARG2-CEBPB	N/A	Replicate 1	Human pluripotent stem-cell derived brown adipose cells	DMSO (after 7 days of induction/differentiation)	N/A
HR1	PSC-BAs (DMSO)_r2	25487280	SRP042186	GSM1396749	ventilated from PPARG2-CEBPB	N/A	Replicate 2	Human pluripotent stem-cell derived brown adipose cells	DMSO (after 7 days of induction/differentiation)	N/A
HR1	PSC-BAs (DMSO)_r3	25487280	SRP042186	GSM1396750	ventilated from PPARG2-CEBPB	N/A	Replicate 3	Human pluripotent stem-cell derived brown adipose cells	DMSO (after 7 days of induction/differentiation)	N/A
HR1	PSC-WAs (DMSO)_r1	25487280	SRP042186	GSM1396736	and differentiated from PPARG	N/A	Replicate 1	Human pluripotent stem-cell derived white adipose cells	DMSO (after 7 days of induction/differentiation)	N/A
HR1	PSC-WAs (DMSO)_r2	25487280	SRP042186	GSM1396737	and differentiated from PPARG	N/A	Replicate 2	Human pluripotent stem-cell derived white adipose cells	DMSO (after 7 days of induction/differentiation)	N/A
HR1	PSC-WAs (DMSO)_r3	25487280	SRP042186	GSM1396738	and differentiated from PPARG	N/A	Replicate 3	Human pluripotent stem-cell derived white adipose cells	DMSO (after 7 days of induction/differentiation)	N/A
HR1	PSC-WAs (JAK3)_r1	25487280	SRP042186	GSM1396741	and differentiated from PPARG	N/A	Replicate 1	Human pluripotent stem-cell derived white adipose cells	JAK3 inhibitor tofacitinib (2 μ M), (after 7 days of induction/differentiation)	N/A
HR1	PSC-WAs (JAK3)_r2	25487280	SRP042186	GSM1396739	and differentiated from PPARG	N/A	Replicate 2	Human pluripotent stem-cell derived white adipose cells	JAK3 inhibitor tofacitinib (2 μ M), (after 7 days of induction/differentiation)	N/A
HR1	PSC-WAs (JAK3)_r3	25487280	SRP042186	GSM1396740	and differentiated from PPARG	N/A	Replicate 3	Human pluripotent stem-cell derived white adipose cells	JAK3 inhibitor tofacitinib (2 μ M), (after 7 days of induction/differentiation)	N/A
HR1	PSC-WAs (SYK)_r1	25487280	SRP042186	GSM1396742	and differentiated from PPARG	N/A	Replicate 1	Human pluripotent stem-cell derived white adipose cells	SYK inhibitor R406 (1 μ M), (after 7 days of induction/differentiation)	N/A
HR1	PSC-WAs (SYK)_r2	25487280	SRP042186	GSM1396743	and differentiated from PPARG	N/A	Replicate 2	Human pluripotent stem-cell derived white adipose cells	SYK inhibitor R406 (1 μ M), (after 7 days of induction/differentiation)	N/A
HR1	PSC-WAs (SYK)_r3	25487280	SRP042186	GSM1396744	and differentiated from PPARG	N/A	Replicate 3	Human pluripotent stem-cell derived white adipose cells	SYK inhibitor R406 (1 μ M), (after 7 days of induction/differentiation)	N/A
HR2	Clone1 (BAT preadipocytes)	25774848	E-MTAB-2602	ERR022178	SVF cells from suprascapular BAT	N/A	Replicate 1	Immortalized human clonal brown preadipocytes	None	N/A
HR2	Clone2 (BAT preadipocytes)	25774848	E-MTAB-2602	ERR022180	SVF cells from suprascapular BAT	N/A	Replicate 2	Immortalized human clonal brown preadipocytes	None	N/A
HR2	Clone3 (BAT preadipocytes)	25774848	E-MTAB-2602	ERR022169	SVF cells from suprascapular BAT	N/A	Replicate 3	Immortalized human clonal brown preadipocytes	None	N/A
HR2	Clone1 (BAT)	25774848	E-MTAB-2602	ERR022176	SVF cells from suprascapular BAT	N/A	Replicate 1	Immortalized and differentiated human clonal brown adipocytes	None	N/A
HR2	Clone2 (BAT)	25774848	E-MTAB-2602	ERR022186	SVF cells from suprascapular BAT	N/A	Replicate 2	Immortalized and differentiated human clonal brown adipocytes	None	N/A
HR2	Clone3 (BAT)	25774848	E-MTAB-2602	ERR022185	SVF cells from suprascapular BAT	N/A	Replicate 3	Immortalized and differentiated human clonal brown adipocytes	None	N/A
HR2	Clone1 (BAT + forskolin)	25774848	E-MTAB-2602	ERR022172	SVF cells from suprascapular BAT	N/A	Replicate 1	Immortalized and differentiated human clonal brown adipocytes	Forskolin (10 μ M, 4 hours)	N/A
HR2	Clone2 (BAT + forskolin)	25774848	E-MTAB-2602	ERR022184	SVF cells from suprascapular BAT	N/A	Replicate 2	Immortalized and differentiated human clonal brown adipocytes	Forskolin (10 μ M, 4 hours)	N/A
HR2	Clone3 (BAT + forskolin)	25774848	E-MTAB-2602	ERR022173	SVF cells from suprascapular BAT	N/A	Replicate 3	Immortalized and differentiated human clonal brown adipocytes	Forskolin (10 μ M, 4 hours)	N/A
HR2	Clone1 (sWAT preadipocytes)	25774848	E-MTAB-2602	ERR022170	SVF cells from subcutaneous WAT	N/A	Replicate 1	Immortalized human clonal white preadipocytes	None	N/A
HR2	Clone2 (sWAT preadipocytes)	25774848	E-MTAB-2602	ERR022181	SVF cells from subcutaneous WAT	N/A	Replicate 2	Immortalized human clonal white preadipocytes	None	N/A
HR2	Clone3 (sWAT preadipocytes)	25774848	E-MTAB-2602	ERR022175	SVF cells from subcutaneous WAT	N/A	Replicate 3	Immortalized human clonal white preadipocytes	None	N/A
HR2	Clone1 (sWAT)	25774848	E-MTAB-2602	ERR022174	SVF cells from subcutaneous WAT	N/A	Replicate 1	Immortalized and differentiated human clonal white adipocytes	None	N/A
HR2	Clone2 (sWAT)	25774848	E-MTAB-2602	ERR022182	SVF cells from subcutaneous WAT	N/A	Replicate 2	Immortalized and differentiated human clonal white adipocytes	None	N/A
HR2	Clone3 (sWAT)	25774848	E-MTAB-2602	ERR022179	SVF cells from subcutaneous WAT	N/A	Replicate 3	Immortalized and differentiated human clonal white adipocytes	None	N/A
HR2	Clone1 (sWAT + forskolin)	25774848	E-MTAB-2602	ERR022177	SVF cells from subcutaneous WAT	N/A	Replicate 1	Immortalized and differentiated human clonal white adipocytes	Forskolin (10 μ M, 4 hours)	N/A
HR2	Clone2 (sWAT + forskolin)	25774848	E-MTAB-2602	ERR022183	SVF cells from subcutaneous WAT	N/A	Replicate 2	Immortalized and differentiated human clonal white adipocytes	Forskolin (10 μ M, 4 hours)	N/A
HR2	Clone3 (sWAT + forskolin)	25774848	E-MTAB-2602	ERR022171	SVF cells from subcutaneous WAT	N/A	Replicate 3	Immortalized and differentiated human clonal white adipocytes	Forskolin (10 μ M, 4 hours)	N/A